Bidirectional Reflectance Measurements of Low-Reflectivity Optical Coating Z302

Deepali Shirsekar

Thesis submitted to the faculty of the Virginia Polytechnic Institute and State University in partial fulfillment of the requirements for the degree of

Master of Science

In

Mechanical Engineering

J. Robert Mahan, Chair
Vinh Nguyen, Co-chair
Brian Vick

December 6, 2018
Blacksburg, VA

Keywords: BRDF, Bidirectional Reflectivity, Radiation Heat Transfer, Z302, Monte-Carlo ray trace method, Reflectometry

Bidirectional Reflectance Measurements of Low-Reflectivity Optical Coating Z302

Deepali Shirsekar

ABSTRACT

Black coatings essentially absorb incident light at all wavelengths from all directions. They are used when minimal reflection or maximum absorption is desired and therefore are effective in applications that require control of stray light. Our motivation stems from the use of black coating Lord Aeroglaze® Z302 in aerospace and remote sensing applications and the desire to support the development of bidirectional spectral models that can be used successfully to predict the performance of optical instruments such as telescopes. The bidirectional reflectance distribution function (BRDF) is an indispensable parameter in the optical characterization of such coatings. The current effort involves investigation of the BRDF of the commercial black coating Aeroglaze® Z302. An automated goniometer reflectometer has been designed, fabricated and successfully used for performing the BRDF measurements of Z302 at visible and ultraviolet wavelengths and at both polarizations. The current contribution involves study of Z302 samples prepared at different thicknesses and by different methods, which provides insight about influence of surface roughness on BRDF of Z302.

Bidirectional Reflectance Measurements of Low-Reflectivity Optical Coating Z302

Deepali Shirsekar

GENERAL AUDIENCE ABSTRACT

When light falls on different materials it undergoes various phenomenon such as reflection, refraction, absorption and scattering. The amount of each phenomenon varies with the optical nature of a material as well as the wavelength and direction of the light. Therefore, understanding the optical properties of materials at various wavelengths of light is necessary for effectively using those materials in specific applications which require light to be efficiently reflected or absorbed. This research studies an optical property known as Bidirectional Reflectance Distribution Function (BRDF) of a black coating called Lord Aeroglaze Z302. Black coatings are materials that ideally absorb almost all light that falls on them irrespective of the light's direction and wavelength. They are used in applications where maximum absorption of light is required. One such application which relates to the motivation for this research is absorbing unwanted light in instruments used in space such as telescopes and radiometers. Z302 is used in the Clouds and the Earth's Radiant Energy System (CERES) instruments developed by NASA. BRDF is an important parameter which gives information about all other optical properties of a surface and can be used to know optical performance of that surface. The current work describes the experiments and an automated device developed, called reflectometer, to measure the BRDF of Z302 at different angles and wavelengths of light. The results are reported for different thickness samples of Z302 coating, and two different wavelengths of light that belong to the visible and ultraviolet spectrum of light.

Acknowledgements

I would first like to thank my advisor Dr. J. Robert Mahan, without whom I would not have been able to pursue my dream of achieving a Master of Science degree in Mechanical Engineering at Virginia Tech. Thank you for welcoming me in the Thermal Radiation Group and providing me with this research opportunity and believing that I could do it. Dr. Mahan has helped me to develop as both a researcher and an individual through his never-ending support, encouragement and guidance.

I would also like to thank Dr. Vinh Nguyen and Dr. Brian Vick for willing to serve on my committee. I am happy to have this team of advisors that have constantly supported my research efforts and been extremely patient and kind in tolerating my mistakes.

A very special thank you to Dr. Vinh Nguyen. I have gained an enormous amount of knowledge and experience in the domain of optics while working with Dr. Nguyen. I am grateful to him for putting in so much effort and time in my work, without which this thesis and my first research publication would not have been possible.

I am extremely grateful to our research collaborators and friends, Dr. Kory J. Priestley and Anum Barki Ashraf of the NASA Langley Research Center for giving me this opportunity and believing in my abilities. They have been crucial in making this research possible and have been a constant source of support and encouragement.

I am most grateful to my parents and family. It goes without saying that I owe everything that I am today to my parents. I love you and I am gifted to have you. They have always been there through thick and thin, and any amount of thanks will fall short in front of their love and support. Thank you for everything.

A big thank you to all my friends at Virginia Tech and those back in India. I have had a memorable experience at Virginia Tech because of them and now they are my extended family.

Table of Contents

List of Tables

List of Figures

Chapter 1

Introduction and Motivation

In this chapter we introduce the topic and basic concepts and terminology associated with this thesis and elucidate our motivation for carrying out the research described.

1.1 Introduction

Black surfaces or coatings are materials that absorb essentially all light incident from all directions at all wavelengths, which is the definition of a **blackbody**: "A blackbody is a perfect absorber of thermal radiation; that is, it absorbs all incident radiation from all directions and at all wavelengths" [1, §2.7]. Such coatings are the preferred choice whenever absorption of light and thus minimal reflection is desired in the application [1, §4.3]. When applied to a surface, black paints or coatings reduce the stray light within an optical system. They are also used where maximum absorption of radiation is required, such as on the surface of a thermal detector. Typical applications include enhanced radiation heat transfer and optical devices. Optical instruments process or analyze light waves through refraction, reflection, scattering, polarization and diffraction. Examples of optical applications involving interior black coatings encountered in everyday life are portable telephone and traditional cameras, telescopes, microscopes, binoculars and opto-mechanical components such as mirror and lens mounts.

Knowledge of the bidirectional optical properties, especially the **bidirectional reflectance distribution function (BRDF),** of these black materials is essential for their optical characterization and performance analysis.

The current effort involves investigation of the BRDF of the commercial black coating **Aeroglaze® Z302** [2], which is referred to as Z302 throughout this thesis. The following sections treat the motivation and objectives in further detail.

Black coatings are used in several applications of general and special purposes. Most of these applications involve control of stray light and therefore affect the performance of the optical system or application where they are used. **Stray light**, in simple terms, can be either light from the source being measured that arrives at the detector following a non-optical path, or light that arrives from the ambient. Stray light can be produced by the optical and non-optical components of a system. It degrades the measurement by increasing the noise and thereby reducing the signal-to-noise ratio (SNR). It also limits the working dynamic range for instruments. Stray light becomes a critical issue in complex optical systems such as spectrophotometers [3] and coronagraphs [4]. Therefore, stray radiation needs to be minimized, and one of the methods for achieving this is application of black coatings to key surfaces. Black coatings minimize reflection through increased absorption in non-optical components such as optical mounts, baffles and structural members. The small percentage of reflected light which does occur should be as **specular** as possible in order to accomplish effective reduction of stray light. This is because specular reflections can be controlled by manipulating geometry while diffuse reflections cannot. Therefore, the specularity of a black material is a major factor when considering it for a given application.

Many black materials have been developed and studied over the past several decades. A detailed review of black materials including Aeroglaze® Z302 and Z306, Martin Black, 3M Black Velvet Nextel paint, black anodize, Astro Black and AMES 24E paint is presented in Persky [5]. These materials have been proposed or used in space-borne infrared instruments, thermal detectors, and blackbody calibration applications. In the cited contribution the use of Z302 in telescope baffles is presented along with a comparison of its BRDF to microgrooved black appliqué from Batelle, and black Kapton appliqué, as shown in Fig. 1.1. Note that here "scatter angle" refers to viewing angle, and the incidence angle is 7.5 deg with a wavelength of 10.6 μm. The specular peaks can be clearly seen for Z302 and Kapton.

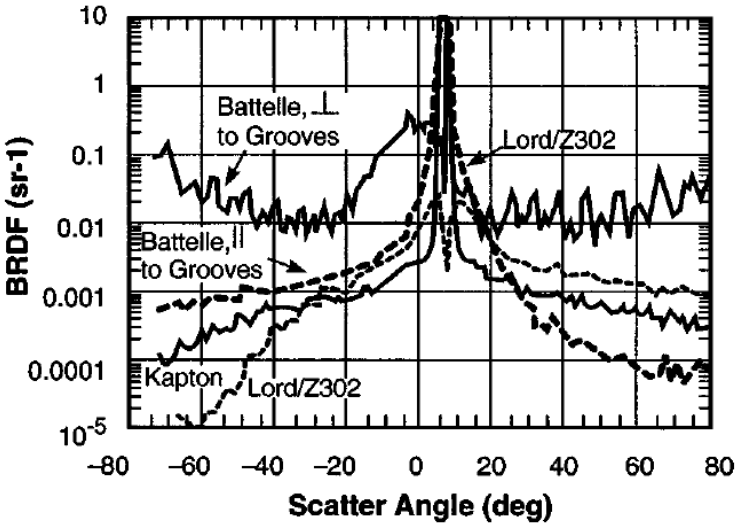

Figure 1.1 BRDF comparison between Lord Aeroglaze® Z302, Batelle, and black Kapton appliqué [5, Fig. 52].

The four primary mechanisms by which low reflectance is achieved are [5]:

1. use of absorbing compounds, such as combining carbon black particles with polyurethane,
2. adding craters or pits larger than the wavelength of light within the surface layer to enable multiple reflections; for example, as in Martin Black,
3. scattering resulting from the surface or substrate structure, which may be diffuse or polished, and
4. optical interference in thin films to enhance absorption.

Table 1.1 lists some of the common black coatings other than Z302 used in the aerospace and optics industries along with their solar absorptivity and normal emittance [6]. This does not mean, however, that every coating or paint that appears black to the human eye is an effective absorber at other wavelengths; absorption depends on the wavelength of the incident light. Therefore, it is important to measure the absorption properties of Z302 at wavelengths other than in the visible spectrum.

Table 1.1 Some common black coatings along with their solar absorptivity, normal emittance and their ratio [6].

Common Black Coatings	Solar Absorptivity, α	Normal Emittance, ε	Ratio, α/ε
Anodize Black	0.88	0.88	1.00
Carbon Black Paint NS-7	0.96	0.88	1.09
Catalac Black Paint	0.96	0.88	1.09
Chemglaze Black Paint Z306	0.96	0.91	1.05
3M Black Velvet Paint	0.97	0.91	1.07
Martin Black Velvet Paint	0.91	0.94	0.97
Polyethylene Black Plastic	0.93	0.92	1.01

1.2 Bidirectional Reflectance Distribution Function (BRDF)

The nature of the interaction between radiation and a surface is not a simple concept. For many problems encountered in engineering, the assumptions of diffuse emission and diffuse-specular reflection are adequate for preliminary analysis in gray enclosures [1, §4.1]. Surface reflectance is generally bidirectional and depends on the mechanical and chemical surface preparation as well as on the wavelength of the incident light. For final design and performance analysis, **bidirectional** surface models are required which depend on the wavelength interval. A bidirectional spectral model for surface reflectance is the most accurate and appropriate tool for such purposes.

The **spectral bidirectional reflectance distribution function (BRDF)**, or **bidirectional spectral reflectivity,** is defined as [7, p. 84],

$$BRDF(\lambda, \vartheta_i, \varphi_i, \vartheta_r, \varphi_r) = \rho''_\lambda = \rho(\lambda, \vartheta_i, \varphi_i, \vartheta_r, \varphi_r) \equiv \frac{di_{\lambda,r}(\lambda, \vartheta_i, \varphi_i, \vartheta_r, \varphi_r)}{i_{\lambda,i}(\lambda, \vartheta_i, \varphi_i) \cos\vartheta_i \, d\Omega_i}. \tag{1.1}$$

In Eq. (1.1), i_λ is the spectral intensity or radiance (W/m^2·sr·μm) of radiation in wavelength interval $\Delta\lambda$, surrounding wavelength λ, $d\Omega_i$ is the incident differential solid angle and the subscripts i and r represent the incident and reflected quantities respectively. These quantities and the remaining symbols in Eq. (1.1) appear in Fig. 1.2. The BRDF determines the intensity $di_{\lambda,r}(\lambda, \vartheta_i, \varphi_i, \vartheta_r, \varphi_r)$ of a beam reflected in direction (ϑ_r, φ_r) from an area element dA due to an incident beam arriving from direction (ϑ_i, φ_i) with intensity $i_{\lambda,i}(\lambda, \vartheta_i, \varphi_i)$. The BRDF is termed "bidirectional" due to its dependence on both the incident and reflected directions. Note that it is not dimensionless, since it is the ratio of reflected intensity to incident power, and therefore has units of sr^{-1} (inverse steradian). The incident radiation beam, though finite, is

restricted to an infinitesimal solid angle, and the reflected beam, scattered in 2π-space, is also an infinitesimal quantity. Therefore, the bidirectional spectral reflectivity itself is a finite quantity. Bidirectional quantities are usually denoted with double prime (″) shorthand notation.

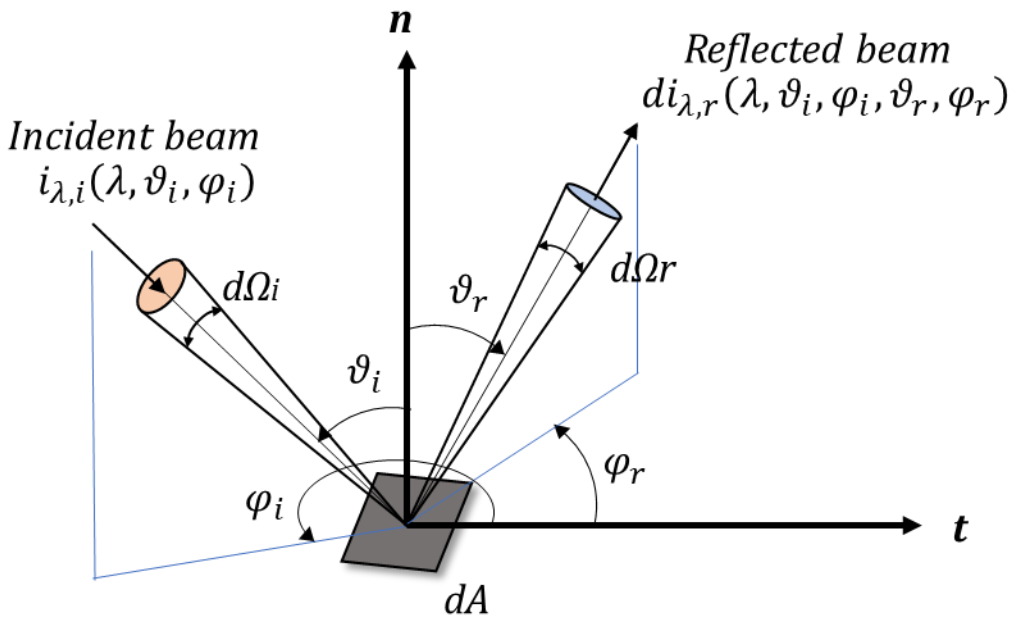

Figure 1.2 Nomenclature for bidirectional reflectivity.

The bidirectional spectral reflectivity, or BRDF, of a surface is a function of wavelength, incident zenith angle, reflected zenith angle and reflected azimuth angle, as indicated in Eq. (1.1). Most surfaces used in practical engineering applications are **isotropic**, which means that the BRDF for these surfaces is independent of the incident azimuth angle. Figure 1.2 shows the manner in which the zenith angle ϑ and the azimuth angle φ are commonly defined in the radiation heat transfer literature. The zenith angle is the angle between the surface normal and the axis of the beam of light, and the azimuth angle is measured from a tangent to the surface

to the projection of the beam axis on the surface. The tangent usually lies in the plane of incidence.

In practice the BRDF of a surface is known to depend on the cleanliness and the chemical, electrical, and mechanical state of the surface, as well as its temperature. For a given coating, it depends on the degree to which it is glossy or matte or a combination of both; therefore, knowledge of the BRDF of a surface provides information about the texture of that surface. Glossy surfaces produce more mirror-like reflections, while matte surfaces produce more diffuse reflections. We know that these two types of reflection represent the two possible extremes; no real-world surface produces 100-percent diffuse or 100-percent specular reflection. Therefore, a physical model for the BRDF is required to quantify the reflection behavior of a surface. Once we know the BRDF for a surface for a given wavelength and incidence angle, we can use it to compute all the other surface properties of that surface (absorptivity, emissivity, and the remaining reflectivities) [7, p. 85]. Therefore, the BRDF is an indispensable parameter in the optical characterization of a surface and provides information about the interaction between radiation and surfaces. It describes the actual behavior of real-world surfaces and therefore is, in principle, superior to the two-component model commonly used in radiation heat transfer analysis [7, p.14].

Apart from remote sensing applications such as Earth scene monitoring and surface mapping, the BRDF is important in remote monitoring of vegetation growth, canopy cover and soil surfaces [8]. In the aerospace industry, knowledge of the BRDF is used for stray light analysis and performance modeling of special paints or coatings. Today, applications of the BRDF have advanced to areas beyond those encountered in real-world optics. The BRDF is used in computer graphics and computer vision algorithms to create realistic images of objects.

Electronic visual displays utilize the BRDF information for performance improvements. It is studied in the energy and solar power sectors to determine and optimize the specularity of reflective components. These data are used in the performance evaluation of solar reflectors and concentrators [9]. BRDF also finds use in defense applications such as ground and air target signature modeling [5].

1.3 Motivation of Current Effort

Stray light control is important in space-borne instruments such as telescopes and radiometers intended to monitor the broadband radiance of the Earth's atmosphere and surface. The data collected from Earth observing systems need to be as accurate as possible. Such systems are extremely sensitive to incident radiation. Our initial interest in Z302 was inspired by its use in the **Radiation Budget Instrument (RBI)** [10], selected and eventually de-selected by NASA as the follow-on for the **Clouds and the Earth's Radiant Energy System (CERES)** instruments [11]. RBI was to be a passive remote sensing instrument aboard the sun-synchronous, JPSS-2 spacecraft to aid with monitoring climate change. RBI's primary goal was to provide measurements of broadband reflected solar radiance and Earth's emitted thermal radiance, over shortwave, longwave and total spectral bands [10]. NASA's attempt to explore the role of clouds in the global climate system and the radiation balance led to the development of CERES instruments as part of NASA's Earth Observing System (EOS). The first CERES instrument launch was in December 1997 aboard NASA's Tropical Rainfall Measurement Mission (TRMM) [12]. For more than 20 years, CERES has provided stable and repeatable Earth Radiation Budget data, valuable in studying the Earth's climate systems and incoming and outgoing energy [12]. Our continuing interest is based on the need for this technology in the eventual follow-on for CERES as well as for CERES itself. NASA has also

developed and utilizes BRDF models for the Earth, based on scene viewing geometry and solar angles, which support satellite remote sensing applications. The Thermal Radiation Group at Virginia Tech was selected to support NASA's effort to build an end-to-end dynamic optical-electrothermal model of RBI, whose performance modeling requires knowledge of the optical performance of Z302.

Several investigations have been carried out based on BRDF measurements for Z302 over different wavelengths; however, the published data often do not include critical information such as sample fabrication details, measurement details, or Z302 layer thicknesses. Prokhorov and Prokhorova [13] made significant early contributions. They present a three-component BRDF model shown in Fig. 1.3 [13], fitted to measured in-plane BRDF data of Z302 at different incidence and viewing angles for a wavelength of 10.6 μm. They then apply the BRDF model in Monte Carlo ray-tracing (MCRT) calculations to predict the performance of a cavity blackbody calibration source. Their effort established a need for mathematical BRDF models, fitted to experimental data, that can be used in the MCRT method. In practice, BRDF measurement is performed at certain angles of incidence and for a discrete set of viewing angles only [13]. However, the MCRT method requires data at all possible incidence and viewing angles, and this need is fulfilled by parametric models which can accurately fill in the missing data.

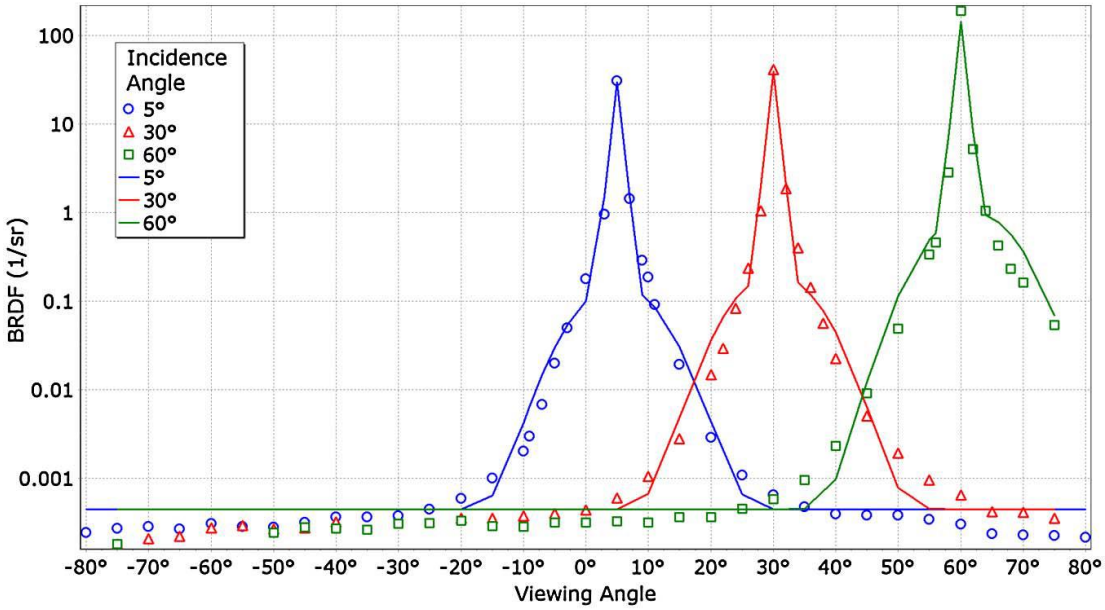

Figure 1.3 Three-component model (lines) fitted to measured in-plane BRDF data of Z302 at 10.6 μm (symbols) [13].

To deal with bidirectional radiant interchanges in enclosures, Mahan, Vinh and Priestley [14] present a four-component BRDF model, based on the Prokhorov and Prokhorova data for Z302 for application in the MCRT method. Reference 1 also demonstrates simulation of BRDF measurement for a coupon coated with Z302, wherein the number of rays traced and detector resolution are shown to be factors that influence the difference between simulated and actual measurement of the BRDF of Z302.

Harris Space and Intelligence Systems [15] has sponsored extensive BRDF test measurements for Z302 at a wavelength of 633 nm in support of NASA's Radiation Budget Instrument (RBI) program. The BRDF of two Z302 coupons (SN1 and SN2) are reported for incidence angles of 5, 35, 55, 70 and 80 deg over a range of viewing angles. The data are used with permission and were measured by Photon Engineering for NASA under a subcontract to

Harris Space and Intelligence Systems. Figure 1.4 shows the BRDF plots for SN1 sample at 633 nm. These datasets proved important for comparison with the BRDF results reported in the current effort. The experimental results in the visible spectrum for the initial Z302 samples described in Chapter 2 are reported in Shirsekar, Wang, Mahan, Priestley and Vinh (2018) [16]. The cited work describes a BRDF model composed of diffuse, glossy and specular components fitted to the measured BRDF data for performance prediction of Z302 on the surface of an actual device such as a telescope.

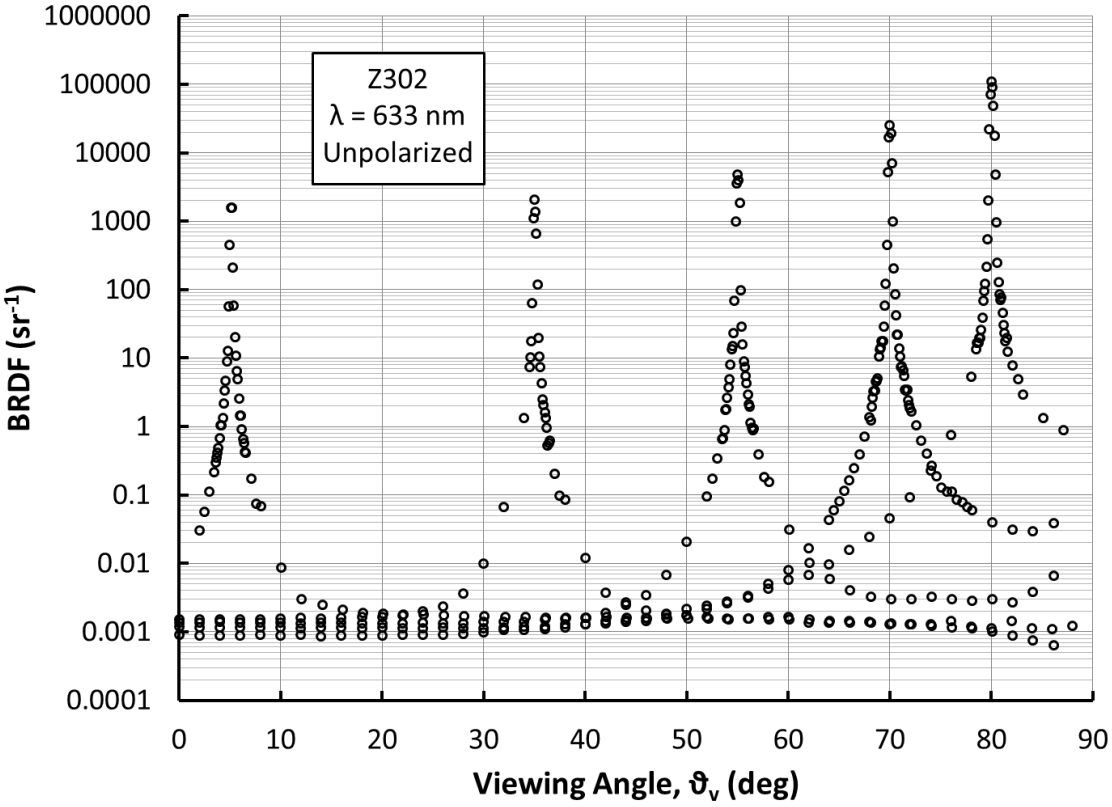

Figure 1.4 Unpublished BRDF measurement results at 633 nm of Z302 provided by NASA [15].

Aeroglaze® Z306 and Z307 are black coatings, also from the LORD product line, that have a matt black finish, compared to Z302 which has a glossy black finish. Advantages of these coatings include good durability, low reflectance in the visible spectrum and high emissivity in the infrared spectrum [17].

1.4 Objectives

The primary contribution of this effort is to provide more specialized data for Z302 in support of BRDF model development. The literature is rather limited in terms of BRDF measurement for Z302 as a function of incidence angle and wavelength [5, 13-15]. The results vary to some degree owing to a combination of errors in measurement and variations between samples. Also, the preparation of Z302 samples with varying thicknesses and the effect of layer thickness on its reflectivity are important aspects that have not been rigorously documented in the literature. The current effort emphasizes these aspects. These data are essential for defining the values of parameters in numerical surface models for use in predicting the performance of a given optical instrument using Z302 as coating. Therefore, the main goal of this effort is to obtain more specialized and complete data for defining BRDF models of Z302.

1.5 Organization

This thesis is organized into five chapters. Chapter 1 introduces the topic and motivation for this work. Chapter 2 defines the surface coating of interest, Aeroglaze® Z302, and discusses the process of creating samples for measuring its performance. Chapter 3 provides the background needed to understand the BRDF measurement methods and the apparatus designed, built and used for this effort. Chapter 4 presents the experimental results for the different BRDF measurements. Finally, the conclusions and recommendations for future work are given in Chapter 5.

Chapter 2

Creation of Aeroglaze® Z302 Samples

Presented is a detailed discussion of the processes used to fabricate the Z302 coatings whose bidirectional reflectivities are the subject of this thesis. The Z302 material properties and handling instructions are also discussed.

2.1 Lord Aeroglaze® Z302

Lord Aeroglaze® Z302 Absorptive Polyurethane Black is a popular and durable coating widely used in aerospace and optical applications for the control of stray light [1, §4.3]. It was originally manufactured and distributed by LORD Corporation [18]. It is often the product of choice because of its high solar absorptivity ($\geq$ 95 percent according to Table 2.1 [2]), depending on the thickness of the coating and the wavelength of incident light. When Z302 is used in an enclosure, stray light propagation can be minimized by using geometry to exploit the fact that reflections that do occur are mostly specular (93 percent at 60 deg of incidence, as shown in Table 2.1). It is also preferred in space applications due to its low rate of outgassing [2], its durability, and its resistance to the effects of aging. It performs well on both rigid and flexible substrates and exhibits mechanical robustness for long durations, as is required for use in autonomous orbital operations.

A relevant concern of using Z302 is that, in its uncured form, it is toxic and hazardous. Inhalation of fumes must be avoided when working with the liquid form of Z302. When handling and during storage, all pertinent instructions in the Material Safety Data Sheet (MSDS) must be carefully observed. Photographs of the one-gallon container of Aeroglaze® Z302 purchased at a cost of more than $900 for this research appear in Fig. 2.1. The plastic safety seal on the lid, which is in addition to the usual friction lid found on common paint cans, is evidently required for shipment of Z302. Also, note the various safety icons and danger warnings in the image on the right in the figure.

Figure 2.1 One-gallon (3.79-l) container of Lord Aeroglaze® Z302 Absorptive Polyurethane Black.

The optical and physical properties of Z302 are provided in Table 2.1. Note the relatively low flash point (16.1ºC) and high level of volatile organic content (618 g/l). The “theoretical coverage” indicates the area in square feet covered by one gallon of Z302, to a one millimeter

dry-film thickness. The normal emissivity specified is measured by a radiation thermometer (R.T.) in the spectral range 5-25 μm.

Table 2.1 Lord Aeroglaze® Z302 properties [2].

Typical Properties of Aeroglaze Z302 Polyurethane	
SOLIDS CONTENT % by weight % by volume	 34 28
DENSITY lb/gallon	 7.8
VISCOSITY, @ 25°C (77°F) cP (thixotropic)	 75
GLOSS, 60° incidence angle, %	93
SOLAR ABSORPTION, Gier-Dunkle Integrating Sphere	≥ 0.95
NORMAL EMISSIVITY (5-25 μm @ R.T.)	0.90 ± 0.02
OUTGASSING, % Total Mass Loss	1.39
FLASH POINT C °F	 16.1 61
VOLATILE ORGANIC CONTENT (VOC) g/liter lb/gallon	 618 5.1
THEORETICAL COVERAGE ft^2 /gallon/mil	 448
COATING FILM DRY WEIGHT lbs/ft^2/mil	 0.0059

2.2 Sample Fabrication Process

Sample fabrication is a crucial part of investigating any material and its properties. It involves the same level of planning and careful execution as any scientific experiment. Thus, the samples reported in this thesis were created after thorough planning and preparation. We achieved good samples only after many trials and errors, learning valuable lessons in the process, as discussed below.

2.2.1 Procurement Of Z302

Lord Aeroglaze® Z302 is a special-order product and is usually available to purchase for a minimum order quantity (MOQ) of 50 gallons [2]. This made procurement of Z302 a difficult and time-consuming task. Manufactured by Lord Corporation, it is now sold by many private vendors. The Aeroglaze® and Chemglaze® product names were acquired by Socomore from Lord Corporation in September 2016 [19]. Fortunately, the Thermal Radiation Group was able to negotiate the purchase of a smaller quantity (one gallon) of Z302 required for our work from Chembar, Inc. [2], but only after contacting and negotiating with many potential vendors (chembar.com, matweb.com, lord.com, Ellsworth Adhesives, Chemical Concepts, chemcenters.com).

2.2.2 Z302 Application Conditions

Lord Aeroglaze® Z302 has a glossy black post-cure physical appearance. When purchased, it is delivered in liquid form and has the appearance of liquid black paint. It should not be applied on damp or wet substrates. The optimum temperature range for application is between 13C (55°F) and 35C (95°F) on clean and dry surfaces [2]. The temperature for application of the substrate must be at least 2.8C (5°F) above the dew point. Z302 cures by reacting with moisture in the

air. Therefore, the cure time and rate depend on the environmental conditions such as ventilation, temperature, and especially relative humidity under which the applied coating is cured. Z302 will eventually exhibit its completely cured properties in about 7 days, in accordance with the acceptable curing conditions shown in the relative humidity-versus-temperature graph, Fig. 2.2 [2]. The slow curing conditions will retard curing rate and rapid curing conditions might cause bubbling.

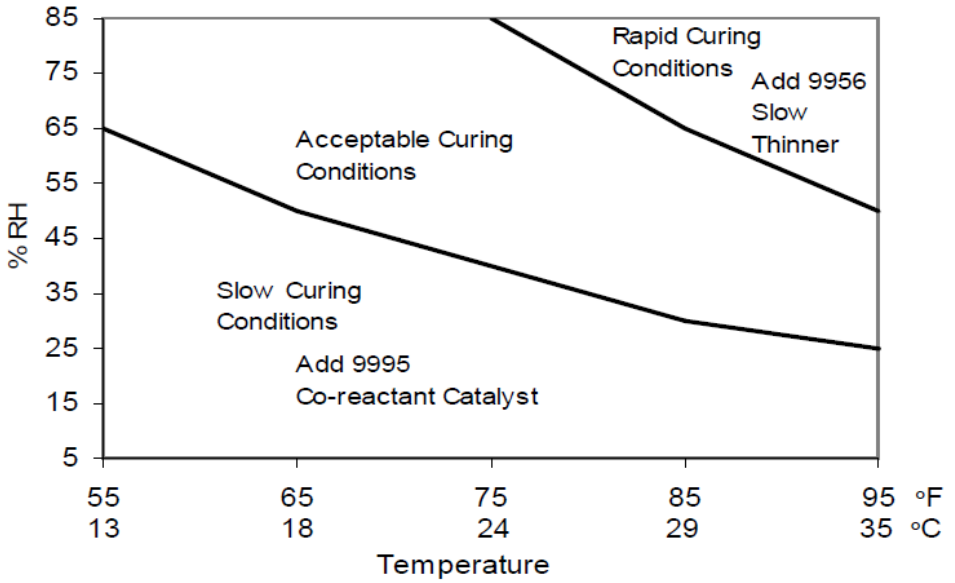

Figure 2.2 Relative humidity (% R.H.)-versus-temperature graph for Z302 curing conditions [2].

The samples prepared for this effort were created and stored by the author of this thesis under the careful supervision of Prof. J.R. Mahan in the well-functioning fume hood shown in Fig. 2.3, located in Optics Laboratory C of the Department of Physics at Virginia Tech, which is directed by Prof. Vinh Nguyen. Necessary personal safety equipment used during handling and application of Z302 were chemical-resistant gloves, a breathing mask, and eye protection.

Figure 2.3 Fume hood used during Z302 sample creation process.

The cure time for safe handling is around 12 h at room temperature and for full normal usage is between 36 and 48 h. The time range for applying a recoat at room temperature is from 3 to 24 h after application of the previous coat. Other information about curing and applying Z302 on any surface can be found in the data sheet provided with the product [2].

The shelf life of an unopened container of Z302 is one year from date of shipment. It is a flammable liquid and so must be stored away from heat and ignition sources. Uncured Z302 degrades in quality with long-term exposure to atmospheric air. This must be kept in mind when working with Z302, and hence it is advisable to transfer small amounts of Z302 from its bulk container into smaller usable containers and work with these. For the current work, this method proved useful in avoiding excessive exposure of the entire Z302 liquid container to air. Once a container is opened, the unfilled portion should be purged with an inert gas, such as dry nitrogen, before resealing it.

2.2.3 Aluminum Substrates

Our initial idea was to coat Z302 on polished thin aluminum substrates due to the good adhesion associated with Z302 on metal. Ten aluminum substrates one-by-one-inch square and having a thickness 0.1 in. were fabricated for this effort, and are shown in Fig. 2.4. They were numbered on the back surface for sample identification and were cleaned using alcohol. Figure 2.5 shows five of the substrates after they were polished using fine emery paper. We soon realized that the surface topography features of the substrate greatly influence the surface topography of the coating unless a thick layer is applied. Measurement of BRDF requires that the surface be uniform and smooth, that surface irregularities be minimized, and that the topography be free of any external bias or influences. Surface features due to polishing can be observed in Fig. 2.5 when carefully observed.

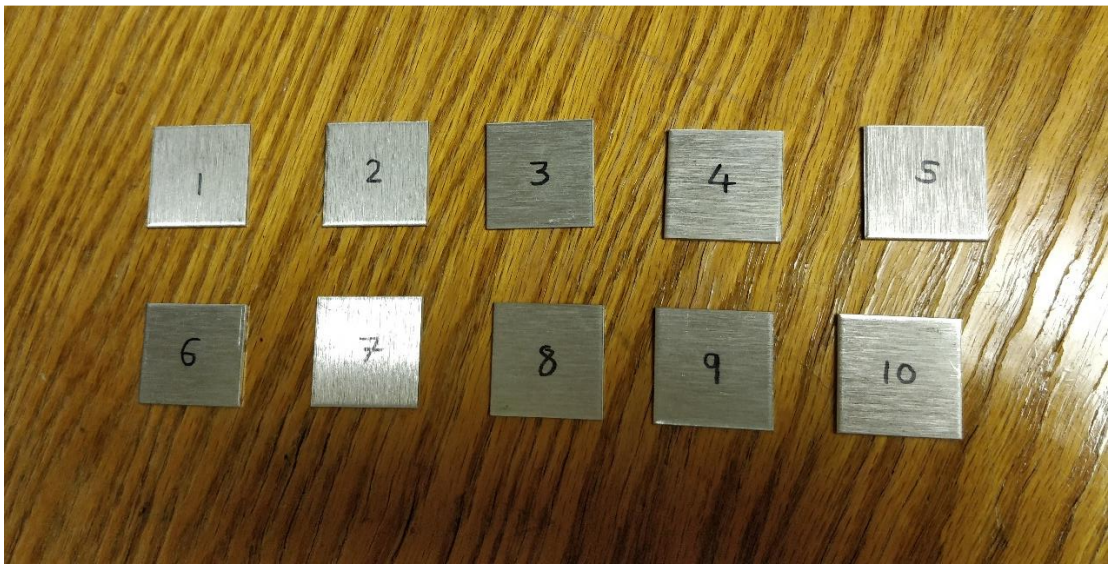

Figure 2.4 Ten aluminum one-by-one inch square substrates (back view).

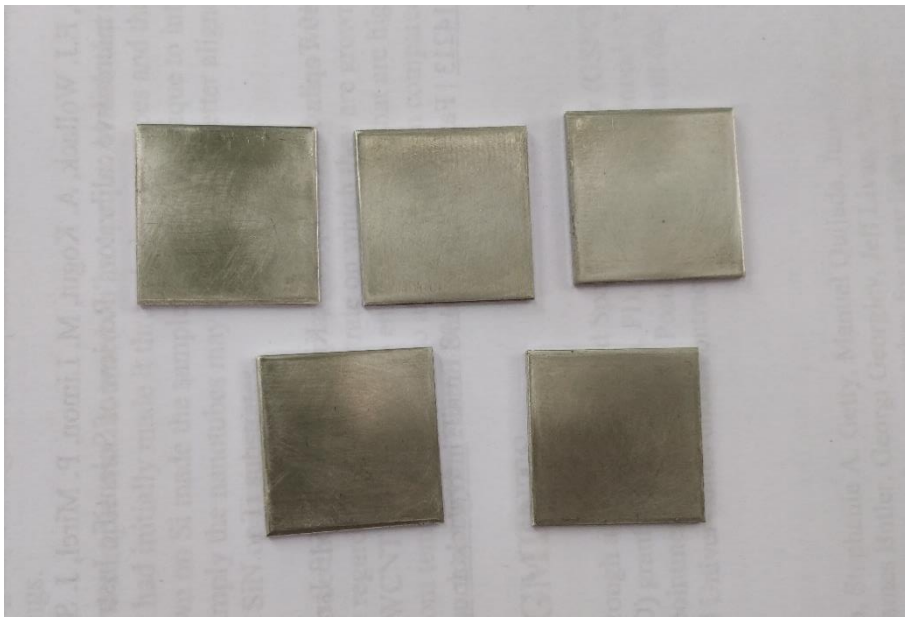

Figure 2.5 Aluminum substrates after being polished with fine emery paper.

2.2.4 Silicon Wafer Substrates and Spray Application of Z302

We reviewed and considered the substrate choices available that were common for such purposes. The desire to have a uniform layer of Z302 was the driving factor for choosing silicon wafers as the suitable substrate. Silicon wafers are sufficiently flat that they do not impose surface features on the subsequent coating, regardless of coating thickness. This promotes repeatability and more meaningful BRDF measurements. The observed reflectivity behavior can be wholly attributed to the nature of the paint or coating itself, and not to the substrate.

The **method of application** of Z302 was the next consideration because it plays a vital role in the uniformity of the coating. Applying a coating manually using a paint brush leads to a final surface topography that retains the shape of the brush bristles; hence, on a microscopic scale the surface will be non-uniform. If done properly the method of spray painting, on the other hand, ensures a uniform distribution of coating droplets and formation of an even coat through the action

of surface tension. Therefore, initially, we used an air-brush with different sized spray-head attachments to spray the uncured liquid Z302 by hand on the silicon wafer substrates. The VL series air-brush kit from Paasche shown in Fig. 2.6 was used for applying the Z302.

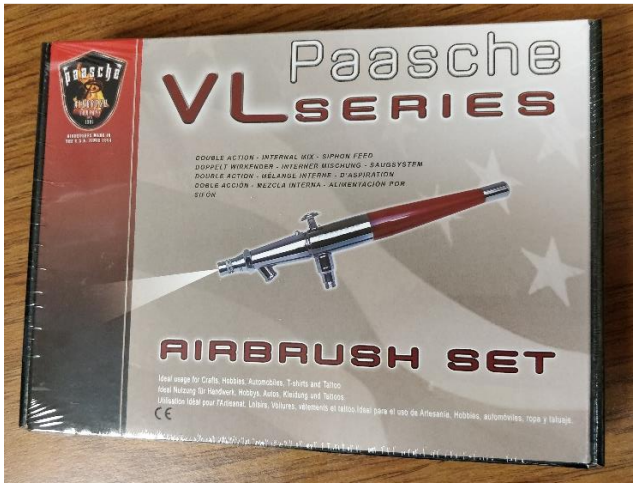

Figure 2.6 Paasche air-brush kit.

Before using the Z302, we decided to practice the hand spraying technique with an ordinary market-available black gloss spray paint. The objective was to practice spraying such that an even layer is achieved on the substrates as well as to obtain experience with controlling the rate and distance of the spray jet of paint. The 400-ml 'Montana White' synthetic spray paint that was used for this activity is shown in Fig. 2.7(a); note that although the name of the paint is 'White', the color is actually black. This paint was hand-sprayed on four of the aluminum coupons shown in Fig 2.5 in an open-air environment, as recommended in the spray can instructions. The substrates were laid out in a straight line over brown paper and the spray nozzle was swept over them, from one end to the other, until about 20 passes were made. The samples were then left to dry in the shade for about 30 min, after which the final coated samples appear as shown in Fig. 2.7(b). Note that spraying with this paint also involved wearing a breathing mask and gloves; all other safety instructions were followed as well.

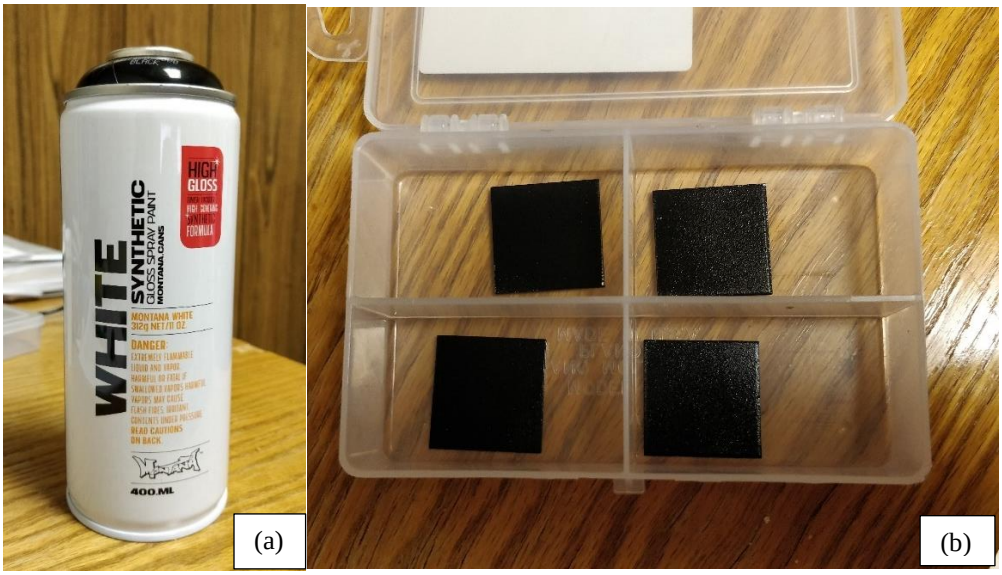

Figure 2.7 (a) **"**Montana White" black gloss spray paint; (b) spray paint-coated dry aluminum substrates.

This proved to be a good exercise for preparing and practicing application of Z302. For example, we learned that the samples must be stored for drying in a dust-free environment because, after drying, the samples in Fig. 2.7(b) had some fine dust particles ingrained in the coat. Also, when spraying a fluid, its viscosity will affect the initial jet discharge, and the starting flow will be inconsistent and lumpy. Therefore, spraying should start not on the surface of interest, but rather in the vicinity of the sample area and then moved slowly towards the sample surface after the spray stabilizes. Another important factor is to maintain the nozzle distance and spray intensity constant. Also, the number of spray passes must be counted to ensure control of sample thickness.

The air brush kit components are shown in Fig. 2.8. They consist of one air brush tool, two bottles (1 oz each) with lids for filling paint, one braided air hose (6-ft length), one metal paint cup attachment (1/4 oz), one airbrush hanger, one wrench for spray head attachment, and three sets of spray-heads, nozzles and spray needles, each set corresponding to a different size. The

head sizes of these sets (not shown in the figure) are 0.55 mm, 0.73 mm and 1.06 mm, and are referred to as size 1, 3 and 5, respectively, in order of increasing spray-cone angle. The size-3 head and nozzle are shown in Fig. 2.9(e).

Figure 2.8 Contents of the opened air-brush kit.

Note that the air-brush kit does not include an air supply, and so separate arrangements must be made for the air supply. For this we purchased a 340-g Paasche air propellant can, shown in Fig. 2.9(a), compatible with the air hose from the kit. A screw-type valve connects the can to the air hose. The air supply components and assembly are illustrated in Fig. 2.9(d) and Fig. 2.9(b) respectively.

(a) (b) (c)

(d) (e)

Figure 2.9 (a) Paasche Air propellant can (340 g), (b) air supply assembly, (c) bulb pipette, (d) air hose, screw-valve and propellant can, and (e) size-3 spray head and nozzle.

Liquid Z302 was first transferred in the fume hood from its original container to the two bottles of the airbrush kit using the bulb pipette shown in Fig. 2.9(c). The staging for this process is shown in Fig. 2.10(a). One of these bottles has a nipple attached to the lid, shown in Fig. 2.10(b),

which facilitates connection to a paint inlet in the airbrush. Figure 2.11 displays the airbrush tool itself.

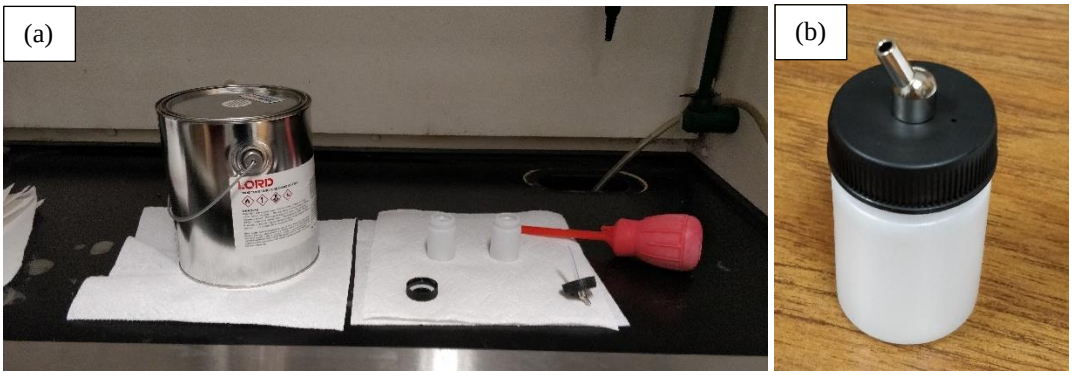

Figure 2.10 (a) Setup for transferring Z302 from its shipping container to the spray bottles using a bulb pipette; and (b) the reservoir bottle with nipple for connecting to the airbrush inlet.

Figure 2.11 Air-brush.

For creating the samples, thirteen vapor-deposited 500-μm thick, silicon wafer square coupons of size 1-by-1 cm were fabricated and used as substrates. These were arranged in a horizontal line on a paper towel in the fume hood, as shown in Fig. 2.12(a). Two of the earlier aluminum substrates were positioned above this line for starting the spray pass. The silicon coupons were affixed to the paper towel using two-sided tape to avoid them being disturbed by

the air spray and hood ventilation system. The airbrush is made operational by connecting the air supply and paint bottle reservoir to its inlets. The air supply is connected to the air brush inlet and then the valve is turned counter-clockwise to initiate flow. The jet from the airbrush is released and controlled using the trigger on top of airbrush, shown in Fig. 2.11. The trigger is simultaneously depressed and pulled rearward for the paint to be released as a spray, with the amount of rearward displacement controlling the paint flow rate.

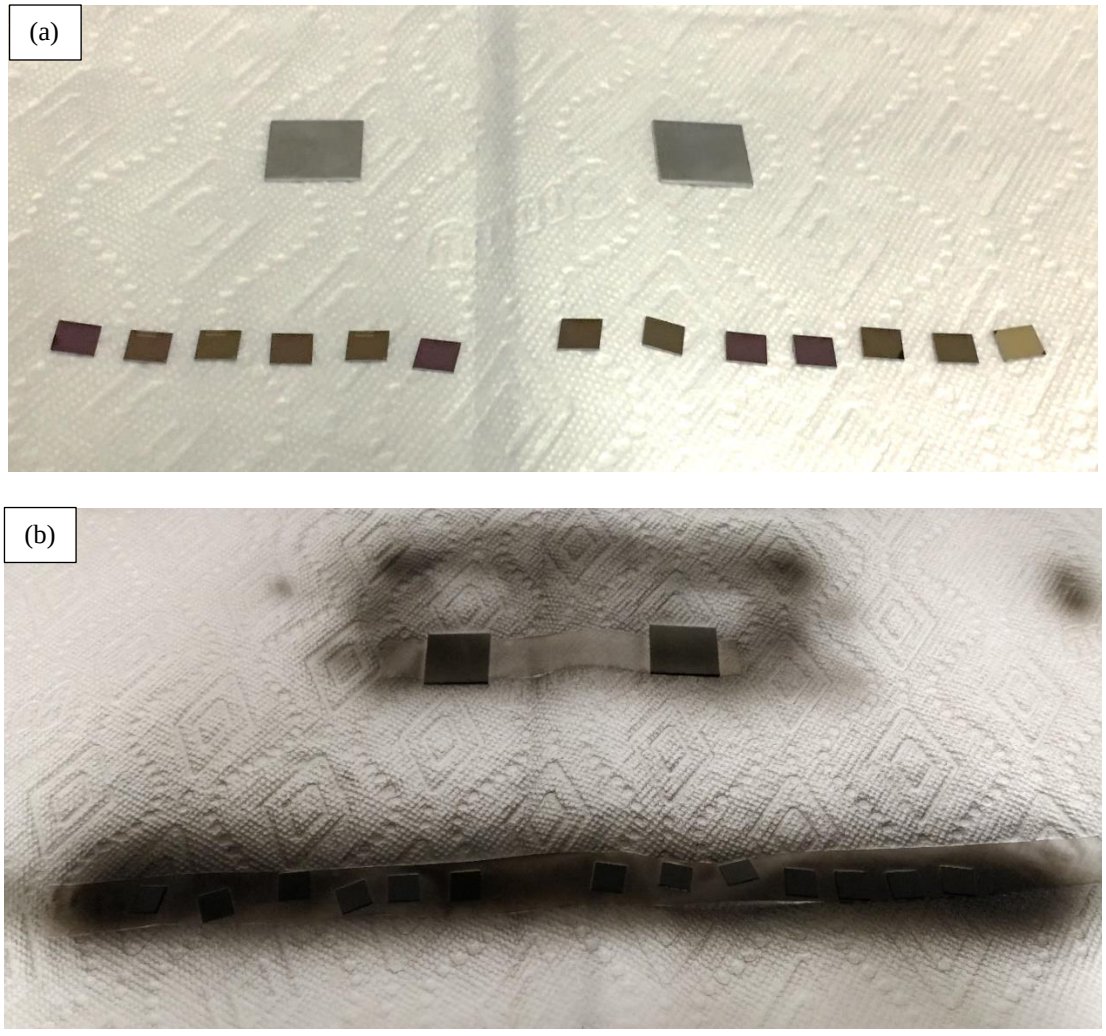

Figure 2.12 (a) Line of silicon coupons with two aluminum coupons placed above them before application of Z302, and (b) the silicon and aluminum coupons sprayed with a single coat of Z302.

The thirteen samples were divided into four groups for performing different numbers of Z302 re-coats on each group, thereby creating sample groups that had different thicknesses. The first three silicon samples in line from the left in Fig. 2.12(a) are Group 1 and these received a single coat of Z302. The next three are Group 2 and received one re-coat (total of two coats) of Z302. The following three were Group 3 and received two re-coats (total of three coats), and the final four were Group 4 and received three re-coats (total of four coats) of Z302. Each coat of Z302 was applied by spraying passes from one end to the other of the line with the number of passes counted. A spray pass was counted once when going from one end to the other. First, 15 spray passes were performed over all 13 samples, which were then left for drying, as displayed in Fig. 2.12(b). This was the first coat and the dry times followed between all re-coats were according to Z302 application instructions described in Section 2.2.2. Then, the first three samples (Group 1) were set aside and the first Z302 re-coat was applied using 17 spray passes on the remaining coupons. These coats were made using the size-3 spray head set in the airbrush. Figure 2.13(a) and Fig. 2.13(b) are photographs of the cured Group 1 and Group 2 samples.

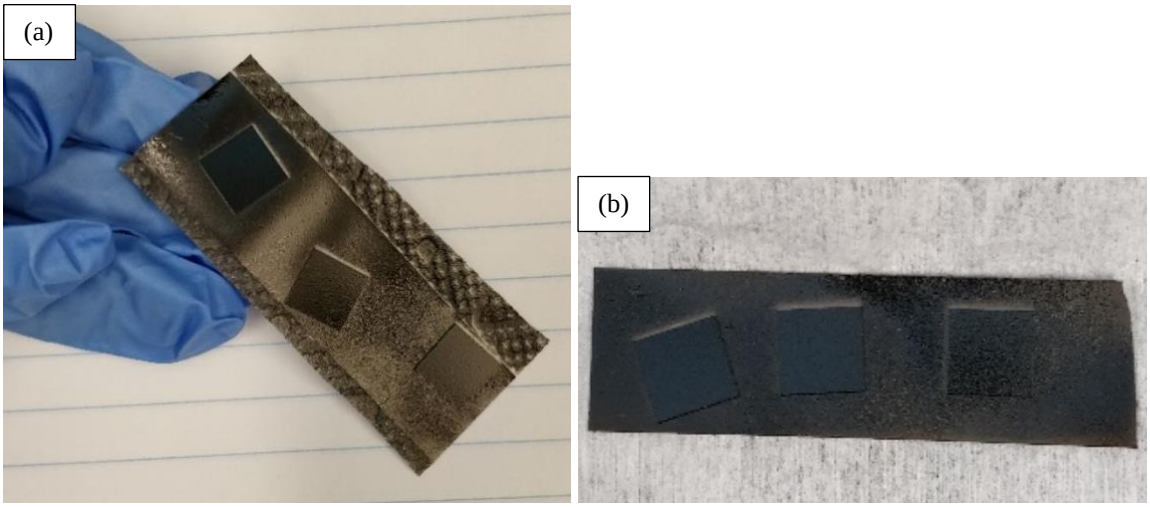

Figure 2.13 (a) Group 1 (single coat) cured Z302 samples, and (b) Group 2 (with one re-coat) cured Z302 samples.

By the time the next re-coat was attempted, the airbrush was no longer operational. This is because it had become clogged with dried Z302 in its flow channels. This is one of the major challenges of working with Z302, apart from its toxicity. When curing, Z302 hardens into a durable solid plastic and is very difficult to remove or clean. The airbrush had to be dismantled and the size-1 spray head and nozzle attached before it was functioning again. The size-3 head, nozzle and needle were solvent-cleaned and allowed to dry.

Finally, after setting Group 2 aside, the author was able to perform a second re-coat by spraying 20 passes on the remaining chips. Figure 2.14 displays the samples after this step. Finally, a third re-coat of Z302 was applied only on Group 4 using 23 spray passes. The spray head was held nearer to the sample surfaces for this re-coat.

Figure 2.14 Group 3 and Group 4 samples sprayed with the second re-coat of Z302.

After allowing the passage of a full normal-usage cure time, around 40 h, all the samples were ready to be handled (wearing gloves) and used without damaging the surface. Figure 2.15 is the photograph of two cured samples, named A and B, from Group 1 and Group 4, respectively [16].

The initial BRDF measurements discussed in the next chapter were performed using these samples. After testing all samples for surface uniformity and smooth BRDF measurements as discussed in detail in Chapter 3, these two samples were found to have the best coating texture from their respective groups. Sample A on the left has a single Z302 coat of 30-µm thickness and Sample B on the right has 95-µm coating thickness consisting of the first coat plus three re-coats of Z302. Clearly, Sample A having a single Z302 layer has a grainier surface texture and appearance than sample B, which appears quite glossy and smooth. Inferences based on the surface roughness are discussed in Chapter 4.

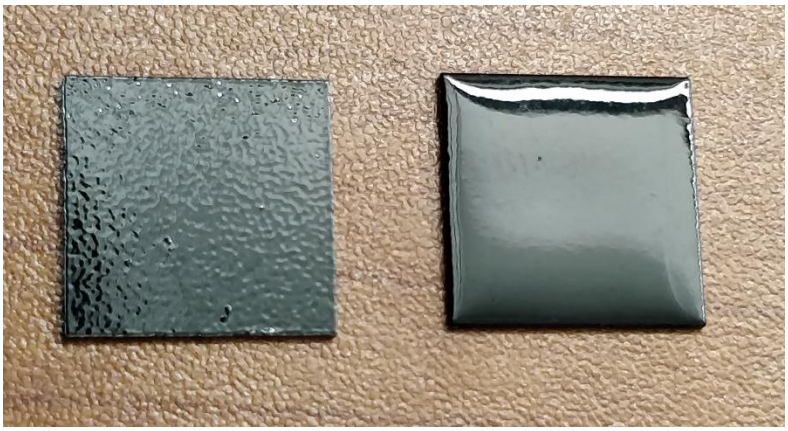

Figure 2.15 Two Z302 samples (A and B). Sample A (left) has a single layer with no re-coats and Sample B (right) has three re-coats [16].

We found that the combination of the spray-head and distance between nozzle tip of spray-head and substrate surface played a crucial role in the quality of the coat. If the spray-head is too fine and/or the distance is too great, the tiny individual Z302 droplets emerging from the nozzle will suffer partial in-flight curing before reaching the surface of the substrate, producing a grainy surface coat. It is imperative for the droplets to arrive at the substrate surface in a liquid form for coalescence to occur and surface tension to act to spread the Z302 uniformly. Figure 2.16 is an

atomic force microscope (AFM) profile image of Sample A. The pits visible on the surface contribute to the diffuse component of reflectivity noted in Chapter 4.

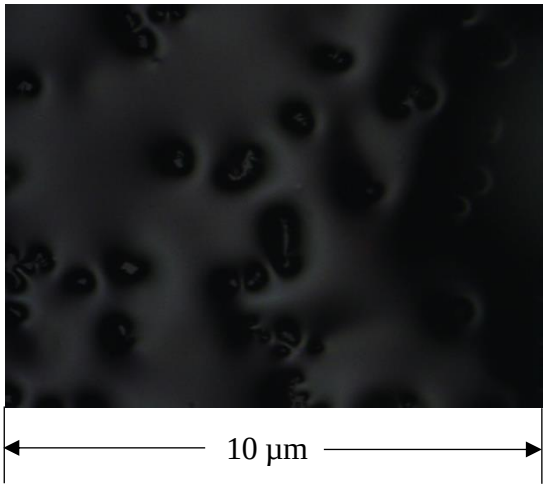

Figure 2.16 Atomic force microscope (AFM) image of Sample A for a 10-µm wide segment.

2.2.5 Glass Slide Substrate and Dipping Method

After conducting BRDF measurements using the samples described above, we decided we needed better samples, gaining from our earlier experience and lessons of the spray application. Again, the post-cure hardness and durability of Z302, which is one of its major advantages, proved to also be a disadvantage. This time the Z302 had dried in the paint reservoir bottles of the airbrush, forming a near-indestructible solid which could not be easily removed. Also, disposal of this toxic waste involves a lengthy bureaucratic process in the University environment. The Z302 residues are shown in Fig. 2.17.

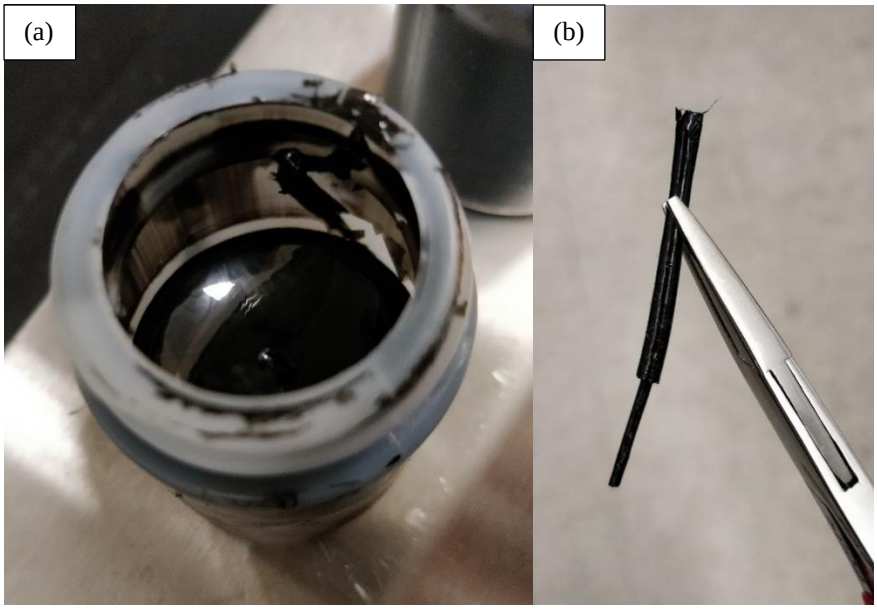

Figure 2.17 (a) Hardened Z302 residue in reservoir bottle and (b) in the gasket tube.

To address this issue, the author discarded the bottles and decided to use the paint cup attachment in the kit shown in Fig. 2.18(a) for spraying Z302. This time the substrate choice included microscope glass slides along with silicon wafers. A few coupons of glass slide and silicon chips were cleaned using acetone, and then spray painted with Z302. Figure 2.18(b) displays the samples created in this attempt. We found that these samples also had local surface variations that became apparent during BRDF measurement. This problem, along with difficulty of cleaning Z302 from clogged airbrush parts, led to serious consideration of another method of applying Z302.

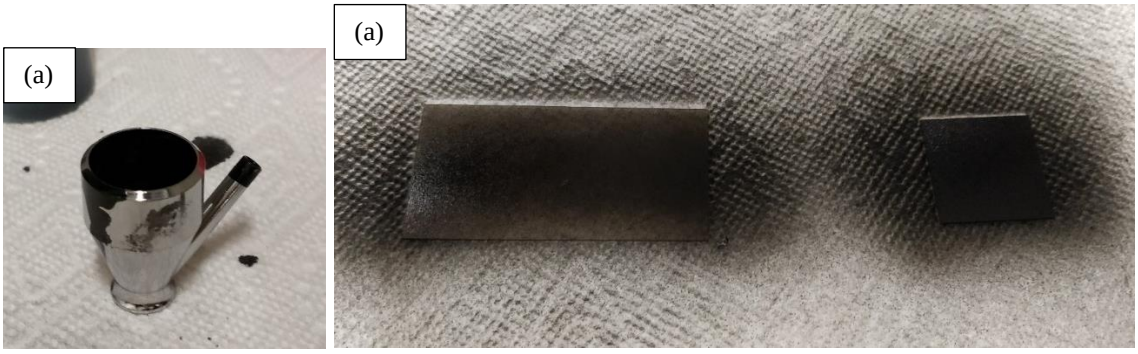

Figure 2.18 (a) Paint cup and (b) new samples on glass slide and silicon chip.

The solution ultimately chosen was to dip the substrates into the Z302 liquid can. This way a locally even coating can be achieved without the need for a means of applying the coating. Figure 2.19 shows the rig built for this method. One glass slide and one round silicon wafer were submerged in the liquid Z302 container with the aid of threads secured at the back face of these substrates. A horizontal orientation was maintained while dipping and drying the samples, as shown in Fig. 2.19. The cured samples appear in Fig. 2.20. The samples in the figure are completely cured although they appear to be wet because of their specularity. The coating layer, which is non-uniform overall, has local patches of uniform thickness which enabled good BRDF measurements. The glass slide sample is named G1.

Figure 2.19 Dipping method rig with samples left for drying.

Figure 2.20 Cured samples created by dipping method; silicon wafer (left) and glass slide, G1 (right)

Chapter 3

The Automated Goniometer Reflectometer and BRDF Measurements

In this chapter we describe the automated goniometer reflectometer that was designed and fabricated in our lab and is capable of measuring in-plane BRDF of not only Z302 but any material sample similar in characteristics and size to the Z302 samples discussed in Chapter 2. Along with the reflectometer, the entire measurement apparatus is explained and our experience with BRDF measurement is presented.

3.1 BRDF Measurement

The measurement of BRDF, traditionally, is accomplished using devices called gonio-reflectometers. These devices use goniometric arms or tables to facilitate the positioning of the light source and detector at different angles with respect to the material sample to be measured. In the approach adopted for these measurements, the light source is kept stationary while the goniometer moves the sample and detector. Therefore, changing the angular position of the sample changes the incidence angle of the light source. Direct BRDF measurement from real materials is difficult, time-consuming and requires precise and well calibrated instruments for

the task. Developing new techniques and devices for this purpose is an active area of research in the radiation heat transfer field.

3.2 The Automated Goniometer Reflectometer

The BRDF measurements of all our Z302 samples were performed using a two-stage automated goniometer reflectometer which is of our own design and fabrication, and is customized according to our project objectives and specifications [20]. Figure 3.1 is the mechanical schematic diagram showing the front view cross-section of only the automated goniometer reflectometer. It is referred to as a "two-stage" reflectometer because it employs two precision rotary stages or motors (these are referred to as just "stages" in opto-mechanical terminology) for performing in-plane BRDF measurements.

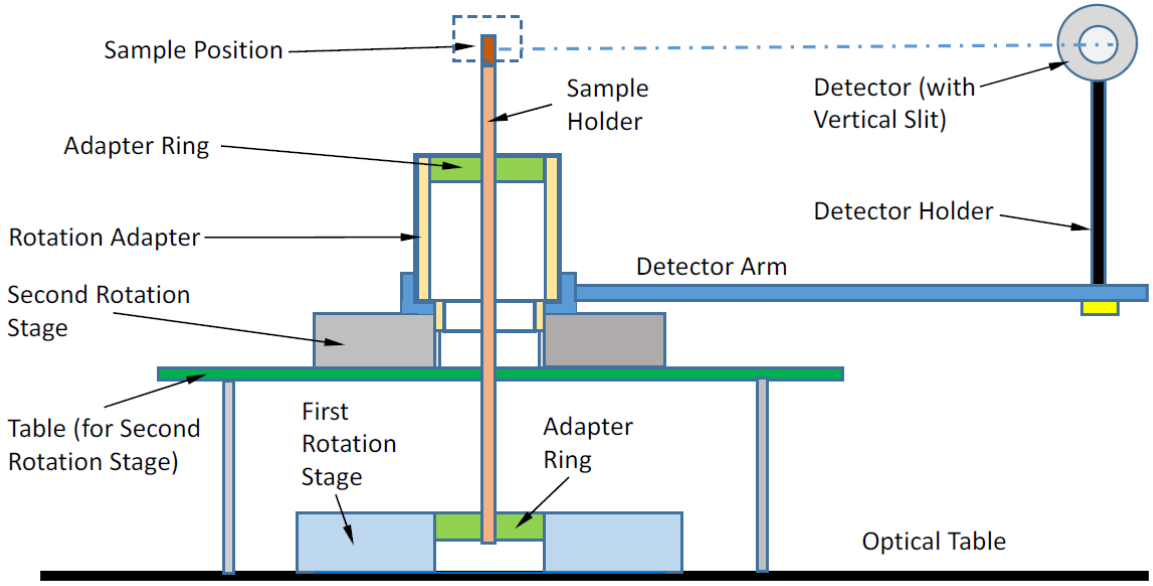

Figure 3.1 Schematic of the automated goniometer reflectometer (not to scale) [20].

3.2.1 Goniometer Design Considerations

After reviewing the literature on BRDF measurements, we decided to design and fabricate a goniometer apparatus that was simple but able to measure in-plane BRDF. As described earlier, only two motor stages are sufficient for this, which minimized apparatus cost and design complexity compared to a three-stage setup (required for out-of-plane BRDF measurements). The design also takes into consideration the available laser equipment in the laboratory, which are fixed to an optical bench. Since the light sources (lasers) for the experiment are fixed, each one of the two motor stages would need to move the sample and detector, respectively. The apparatus also needed to be capable of mounting on an optical table using as little area as possible. The apparatus consists of components designed keeping in mind component strength and stiffness requirements as well as manufacturability in the Physics department machine shop. One important aspect is to design for minimum vibration in both static and dynamic operation. This is especially crucial when the sample to be measured has local variations on the surface over a range of a few micrometers. The parts should also be easily assembled without the need for special tools.

3.2.2 Component Design and Fabrication

With the above considerations in mind, a coaxial goniometric design was conceptualized. Operation of the assembly is illustrated in Fig. 3.2 [21]. Since the goniometer is customized to meet our specific measurement needs, not all components were readily available requiring that the following components had to be designed and fabricated:

1) a mounting table (Fig. 3.3) for the second motor stage,

2) a sample holder (Fig. 3.4) that is capable of transferring motion from the first motor stage,

3) a mechanical arm (Fig. 3.5) that would hold a detector and transfer motion from the second motor stage.

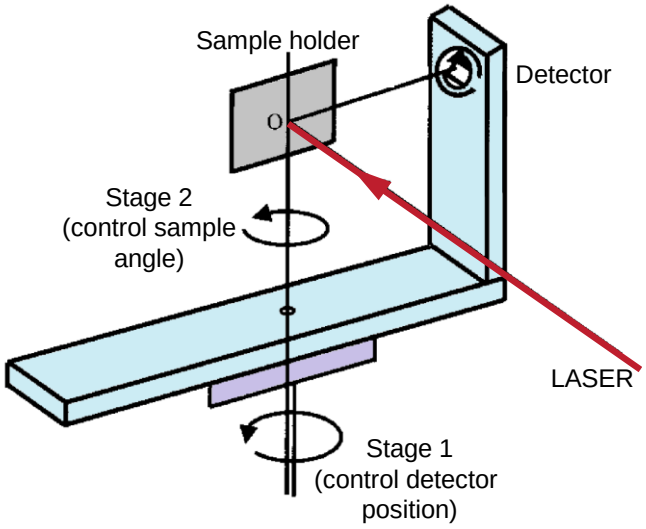

Figure 3.2 Working of a coaxial automated goniometer [21].

These parts were designed in Autodesk® FUSION 360 computer aided design (CAD) software. The three-dimensional CAD renderings of the components can be seen in Figs. 3.3, 3.4 and 3.5. The corresponding two-dimensional shop drawings generated from these are shown in Figs. 3.6, 3.7 and 3.8. All components were fabricated from aluminum in the Physics Department machine shop at Virginia Tech.

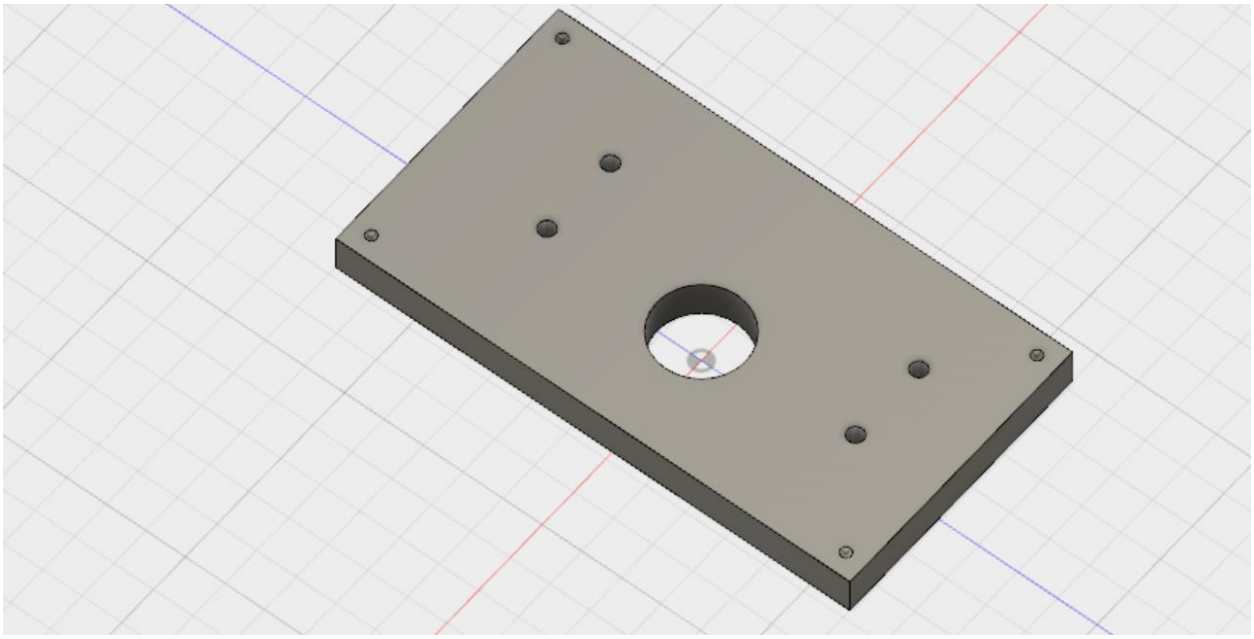

Figure 3.3 Isometric model of mounting table.

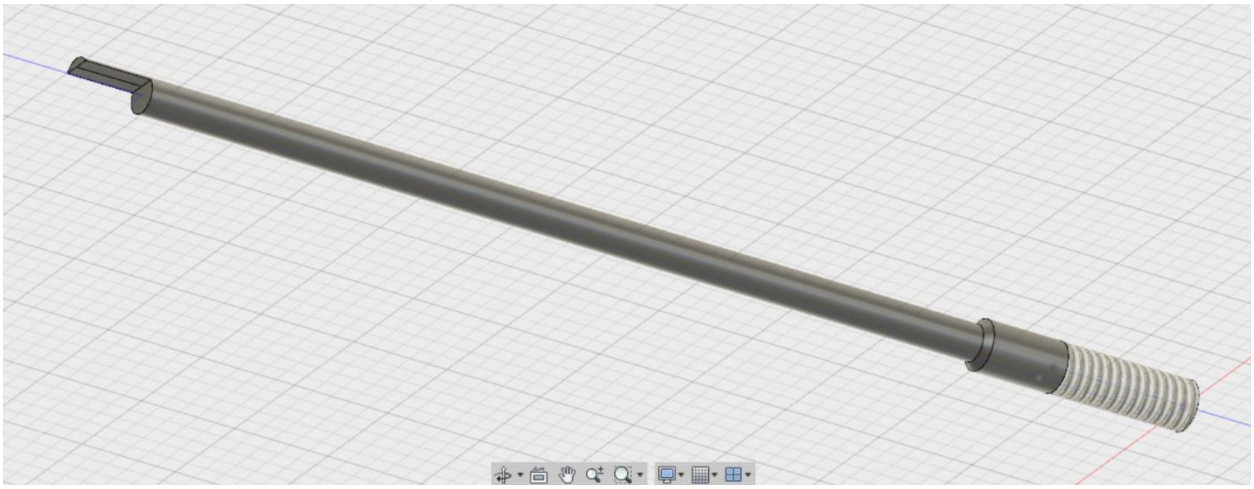

Figure 3.4 Isometric model of sample holder stick.

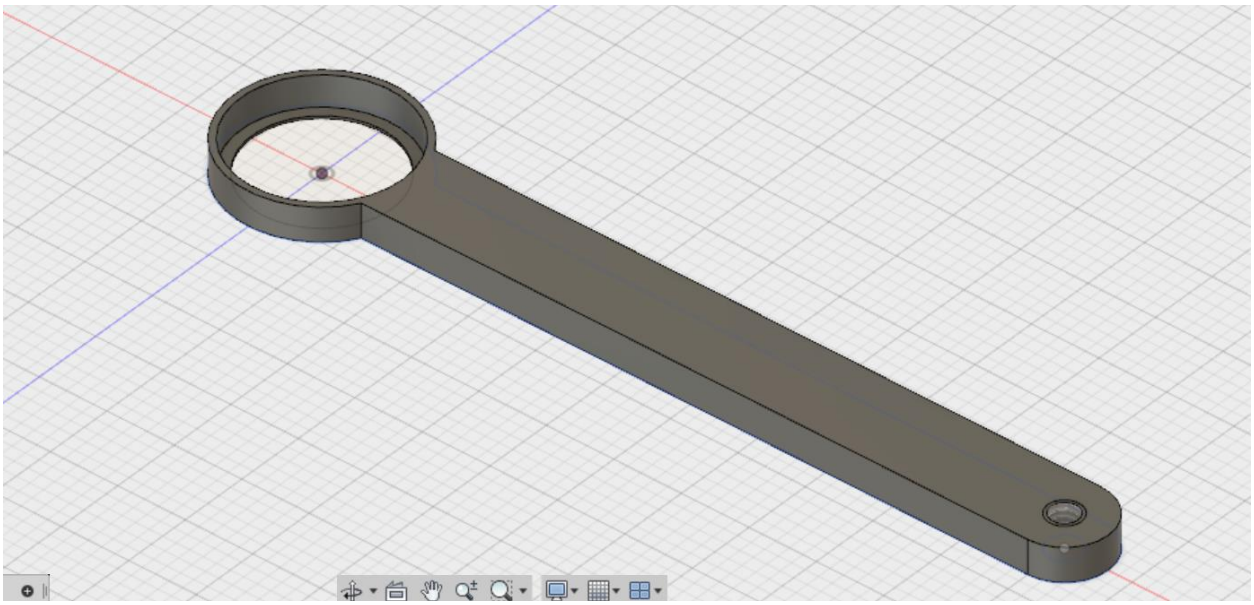

Figure 3.5 Isometric model of detector arm.

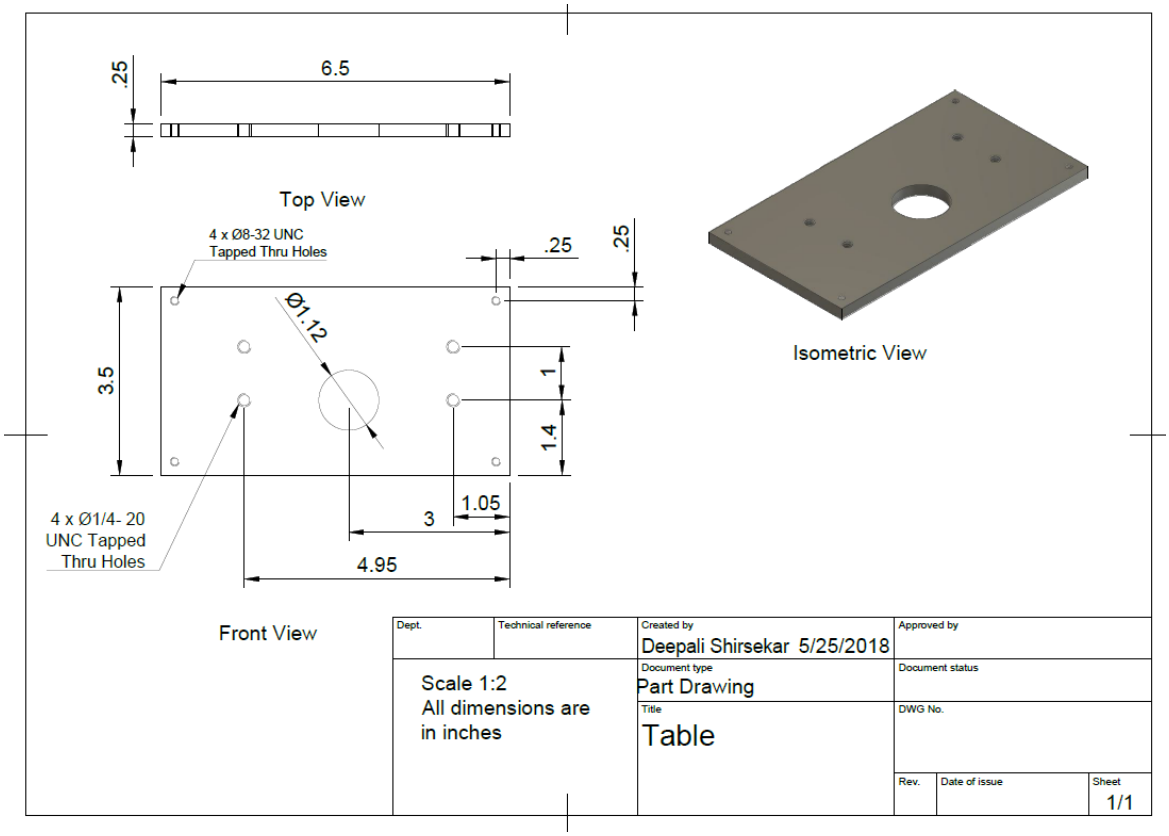

Figure 3.6 Shop drawings of mounting table.

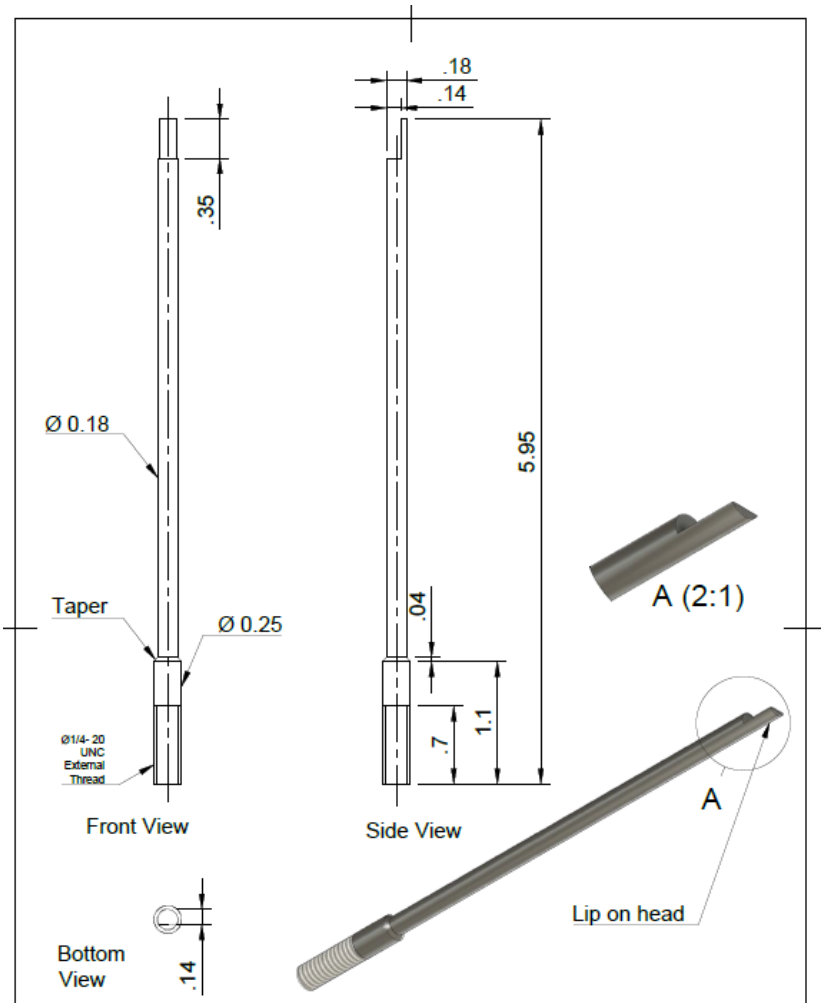

Figure 3.7 Shop drawings of sample holder stick.

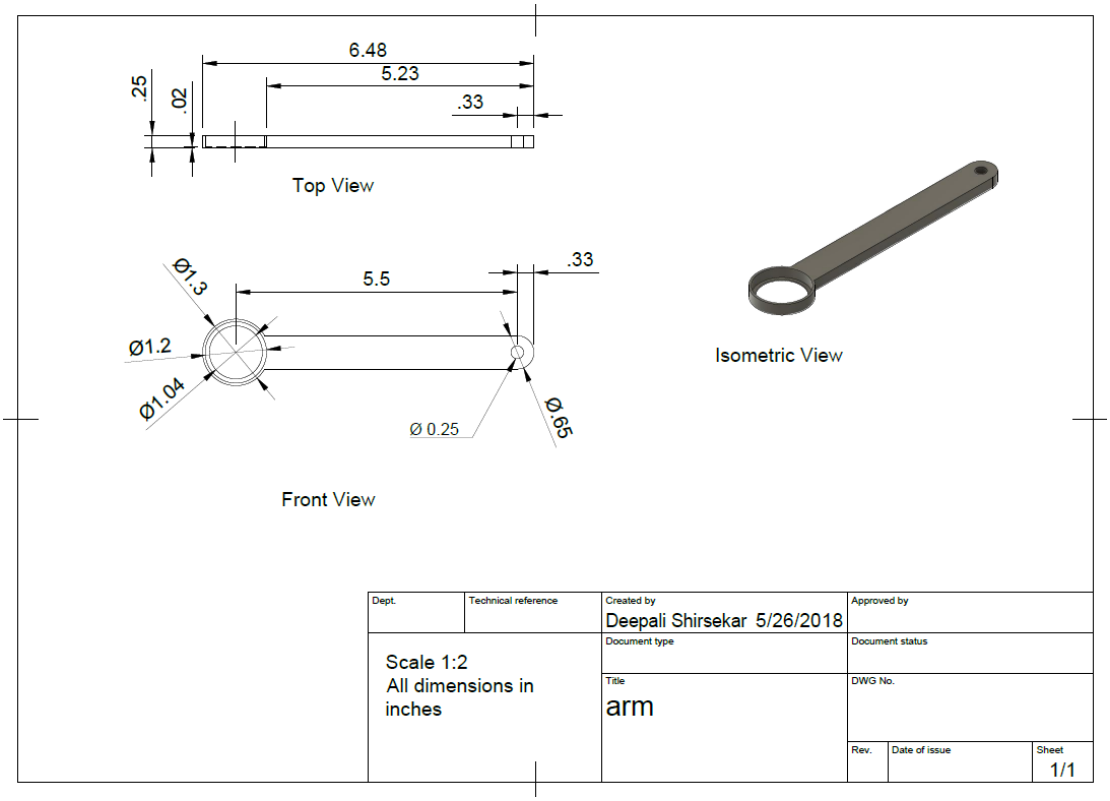

Figure 3.8 Shop drawings of detector arm.

3.2.3 Goniometer Operation

The goniometer is assembled in a coaxial arrangement of the two precision stages, as illustrated in Fig. 3.1. The first stage is mounted on an optical table using fasteners and the second stage is mounted coaxially on the aluminum mounting plate shown in Fig. 3.3. This plate is held in position by securing it to four optical posts as legs. These posts are also connected to the optical table using fasteners. Both rotary precision stage motors are interfaced with LabVIEW software and controlled using a suitable code written for this application. The program sends signals to the stages for angular rotation and also logs their angular position and output of the Newport 918-UV photodetector on a real-time basis. The first rotation stage motor (Stage 1) rotates the sample holder stick shown in Fig. 3.4, which carries the sample.

This rotation varies the angle of incidence of the laser beam on the sample. Therefore, the first stage is commanded manually via LabVIEW to rotate the sample to a specified incidence angle. The incidence angles range from 0 to 90 deg for the measurements described here. The second rotation stage motor (Stage 2) is responsible for rotating the arm on which the photodetector is mounted, shown in Fig. 3.5, to the desired viewing angles. This stage is therefore pre-programmed to rotate the photodetector to a set of specified discrete viewing angles. The samples are illuminated by different laser sources discussed elsewhere. As mentioned earlier, these laser sources are stationary, and therefore rotating the sample changes the angle of incidence of the beam. The photodetector then orbits around the sample in the plane of incidence and senses the reflected intensity in that plane. In this way a coaxial rotation is achieved between the sample and detector.

Two adapter rings are used to ensure proper vertical alignment of the sample holder stick. These were ordered from Thorlabs with product name "SM1A62 – Adapter". One ring is internally fastened to the threaded portion of Stage 1, and the other ring is attached in a similar way to a rotation adapter, whose end is threaded into Stage 2. All of these components are ensured to be coaxial during assembly as indicated in Fig. 3.1. The sample holder stick is then threaded into the bottom adapter ring, and thus motion is transferred to it from Stage 1. The upper adapter ring has a sliding fit with the sample holder stick. The photodetector is fastened to the detector arm and this arm is press fitted to the rotation adapter. Thus, the rotation adapter fulfills two purposes; the first being securing the detector arm in place and transferring motion of Stage 2 to it with the aid of friction, and second to align the sample holder in an upright position. Figure 3.9 is a photograph of the goniometer apparatus, and Fig. 3.10 is a photograph of the first motor stage with the sample holder threaded to its center. This arrangement is below

the mounting plate and hence is not visible in Fig. 3.9. Figure 3.11 is a photograph of the goniometer assembly in operation with the photodetector and silicon coupon in place. Based on successful execution of the measurements and obtaining the satisfactory results reported in Chapter 4, we are confident of the universal applicability of this reflectometer for measuring the BRDF of any coating whose sample is similar in size to our Z302 samples.

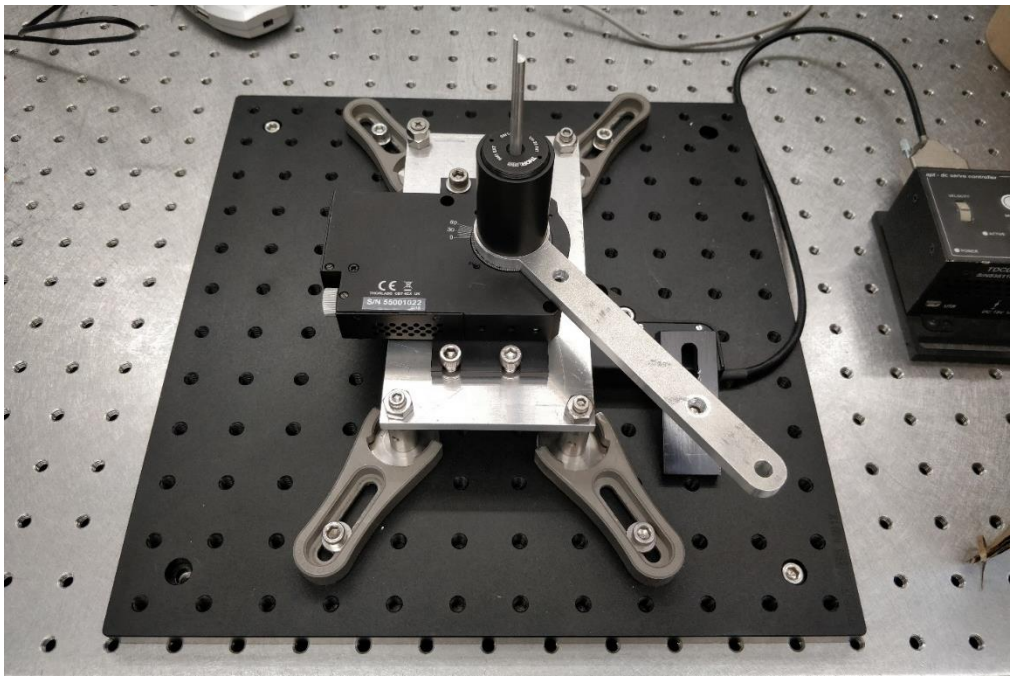

Figure 3.9 Photograph of the goniometer arrangement.

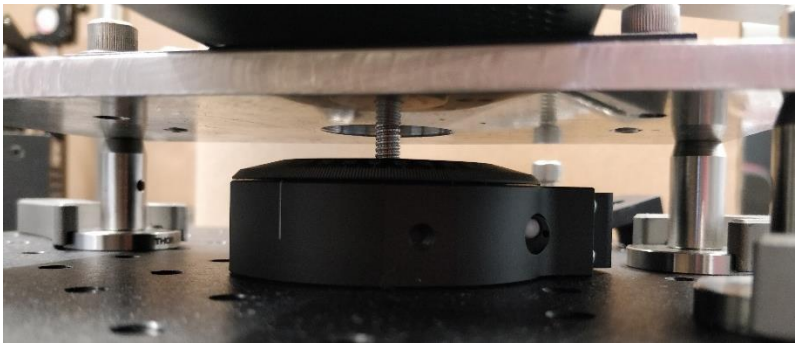

Figure 3.10 Photograph of the first motor stage (not seen in Fig. 3.9).

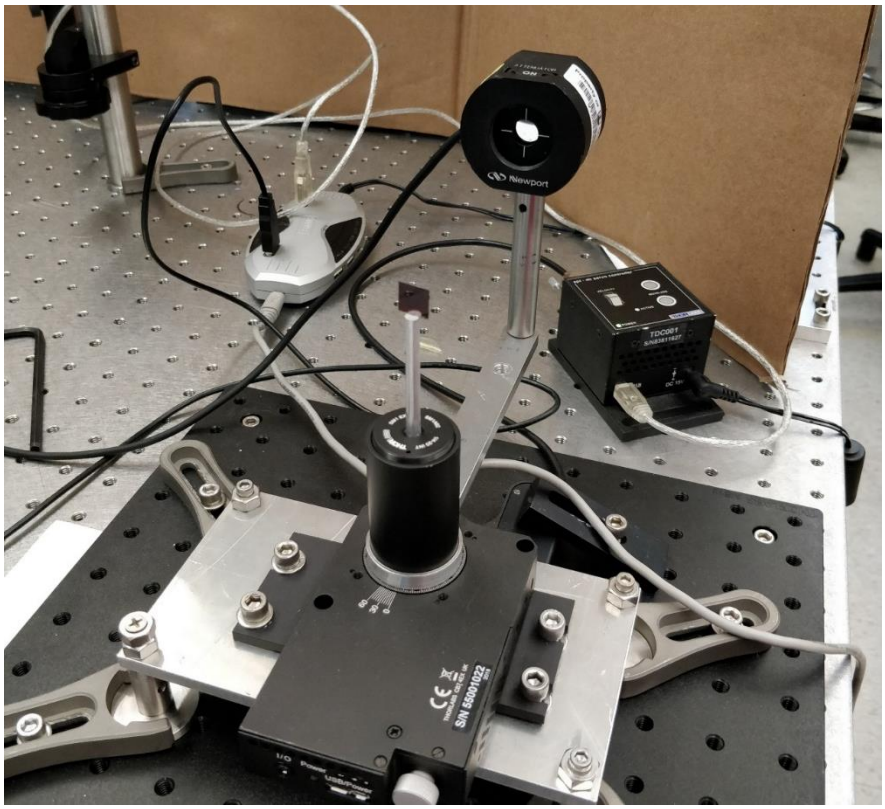

Figure 3.11 Photograph of the goniometer assembly with bare silicon coupon glued to the sample holder and photodetector mounted.

3.3 Experimental Apparatus

The BRDF measurements and experiments were performed in the Advanced Optics Lab directed by Dr. Vinh Nguyen of the Physics Department at Virginia Tech. The measurements were performed using three laser sources which cover the visible, ultraviolet and infrared spectral ranges. The intensity and polarization of the incident laser beams are controlled using a combination of a half-wave plate and a polarizing beam splitter. A 200-μm slit is mounted using aluminum tape as a field stop to the entrance aperture of a Newport 918-UV photodetector. This detector can be used for both visible and UV light detection. The area of this slit is crucial as it determines the solid angle of the reflected beam for the measurements. Calibration of the power

of the beam incident to the sample is done by first reading its known power using a power meter. After this the beam arriving on the sample, along the optical path of the laser, is observed. The design, fabrication and alignment of this reflectometer using a green (visible) laser as the incident light source are described in Reference 16. The following sections briefly describe alignment and use of the apparatus.

3.3.1 Iris Diaphragms

Iris diaphragms, shown in Fig. 3.12, are used to meter the light beam transmitted to an image plane through a circular central aperture. This aperture can be increased or decreased in size by adjusting a lever that operates a set of smooth thin leaves that form the aperture. These leaves are usually made of spring steel. This limits ambient light and narrows a laser beam and is therefore used for aligning purposes.

Figure 3.12 Newport ID-1.0 model iris diaphragms used in the measurements for aligning laser beams.

3.3.2 Chopper and Lock-in Amplifier

Optical choppers are electro-mechanical shutters which interrupt a light beam periodically. They are used in optics laboratories usually in combination with lock-in amplifiers. Their main functions are to modulate the intensity of a light beam and to eliminate the effects of ambient light fluctuations. The three main types of choppers are [22]:

a) variable-frequency rotating disc choppers,

b) fixed-frequency tuning fork choppers,

c) optical shutters.

The chopper used in our measurements is a rotating disc type. The shutters are incorporated in a rotating disc arrangement, as shown in Fig. 3.13. The lock-in amplifier provides feedback to the chopper control. The chopping frequency selected should be as high as possible in order to avoid flicker, or 1/f, noise occurring in electronic devices. The number of slots in the disc, diameter of the beam of light, and motor speed determine the chopping frequency.

Figure 3.13 A rotating disc chopper [23].

A unique aspect of our measurements is that they were conducted in an open environment with the laboratory ambient lights illuminated. This is possible because of the use of the chopper. The chopper attenuates the power of the incident beam and, in conjunction with a lock-in amplifier, removes the background noise and fluctuation effects of lighting from the signal sensed by the photodetector. It is this second function of the chopper that enables us to take measurements with ambient lighting illuminated. Figure 3.14 displays the role of the chopper and its interconnection with a lock-in amplifier.

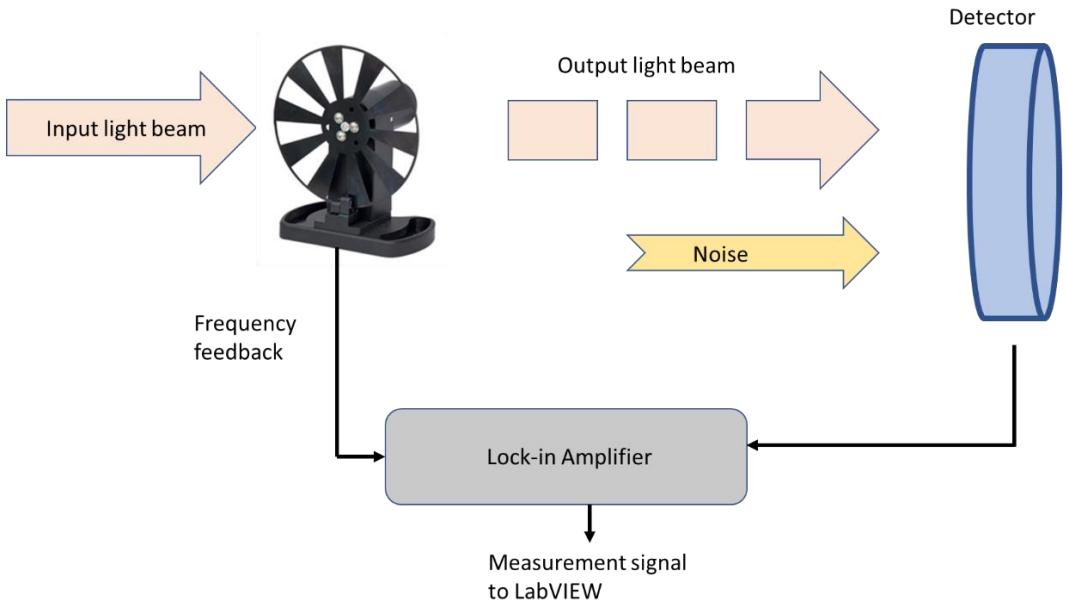

Figure 3.14 Interconnection between chopper, lock-in amplifier, and detector.

A lock-in amplifier is an instrument used to effectively extract signals from noise, even when their frequencies are nearly the same [24]. Accurate measurements are possible, even for very small-amplitude time-varying signals which otherwise would go undetected due to noise of much higher amplitude. The principle of lock-in amplifiers is based on phase sensitive detection. This detection technique extracts a signal component at a specified reference

frequency and phase. This allows elimination of noise signals which are at frequencies other than the reference frequency.

3.3.3 Steering mirrors

Beam-steering mirrors, shown in Fig. 3.15, are used to guide the beam in the desired direction. They are used in combination with one or more iris diaphragms to align a laser beam to the exact spot desired on an image plane. The two control knobs seen on each steering mirror are used to adjust the mirror angle along the horizontal and vertical axes.

Figure 3.15 Steering mirrors.

3.3.4 Periscope

The incident laser beam needs to arrive on the sample surface parallel to the table top in a perfectly horizontal manner. The vertical height of the laser beam is adjusted using a periscope which consists of two flat mirrors mounted one above the other, as shown in Fig. 3.16. The design also allows the light beam to be guided in any possible direction. One mirror is positioned at the height of the laser source and other mirror is positioned at the desired height of the laser beam. Note that these mirrors are intended for use only within specified wavelengths. Therefore, different periscope mirrors were used for visible and UV BRDF measurements.

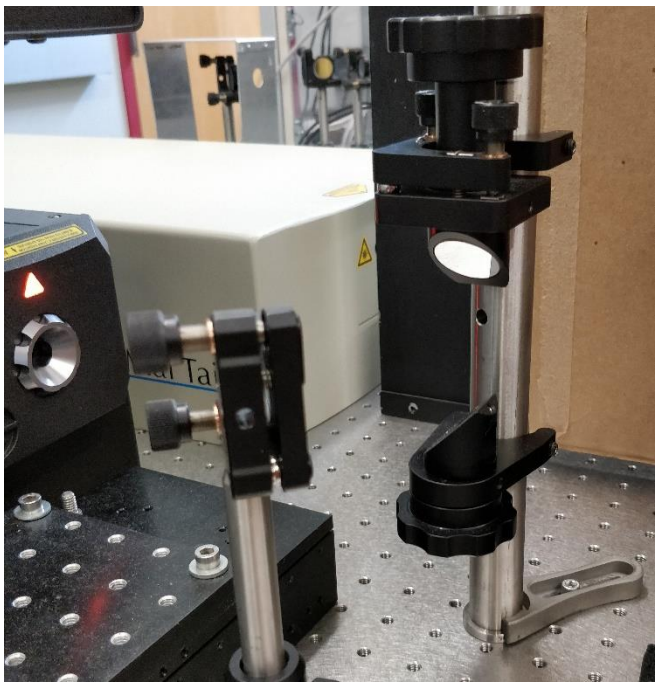

Figure 3.16 The periscope for changing the vertical height of the laser beam.

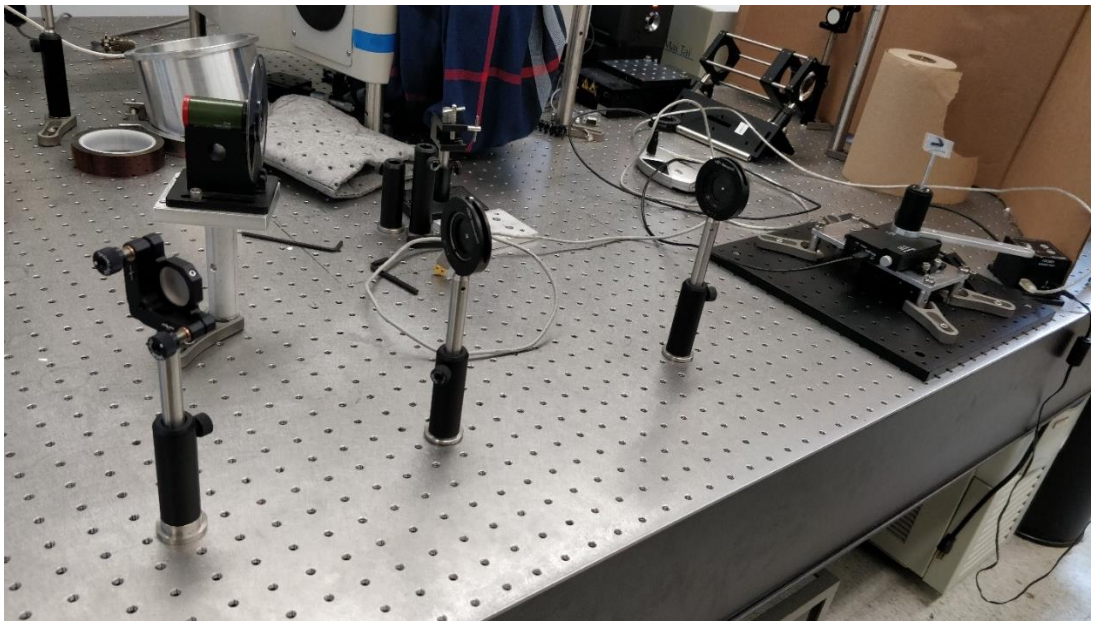

Figure 3.17 Alignment and calibration of the laser beam.

3.4 BRDF Measurements using the Visible Laser (532 nm)

The Z302 samples are illuminated at their center by a power-stabilized 532-nm (green) diode laser. Figure 3.18 is a schematic diagram showing the entire experimental functions (optical and electronic) employed to perform the visible-spectrum BRDF measurements. The red arrows in Fig. 3.18 represent the incident laser beam. The visible (green) beam from the laser source falls on the lower mirror of the periscope from whence it is guided to the upper mirror. This places the laser beam in a horizontal plane at the height of the center of the sample. The beam then falls on the first steering mirror and passes through the center of the half-wave plate and the polarizing beam splitter cube, after which it falls on the second steering mirror. The reflected beam from the second mirror falls on the sample center after first passing through a converging lens. The beam from the second steering mirror to the sample is aligned using

two irises such that it falls on the center of the sample. These two irises are removed during actual measurements. The time required to obtain a typical data set is about 17 to 20 minutes for a particular angle of incidence and corresponding set of viewing angles, depending on the degree intervals chosen for data collection.

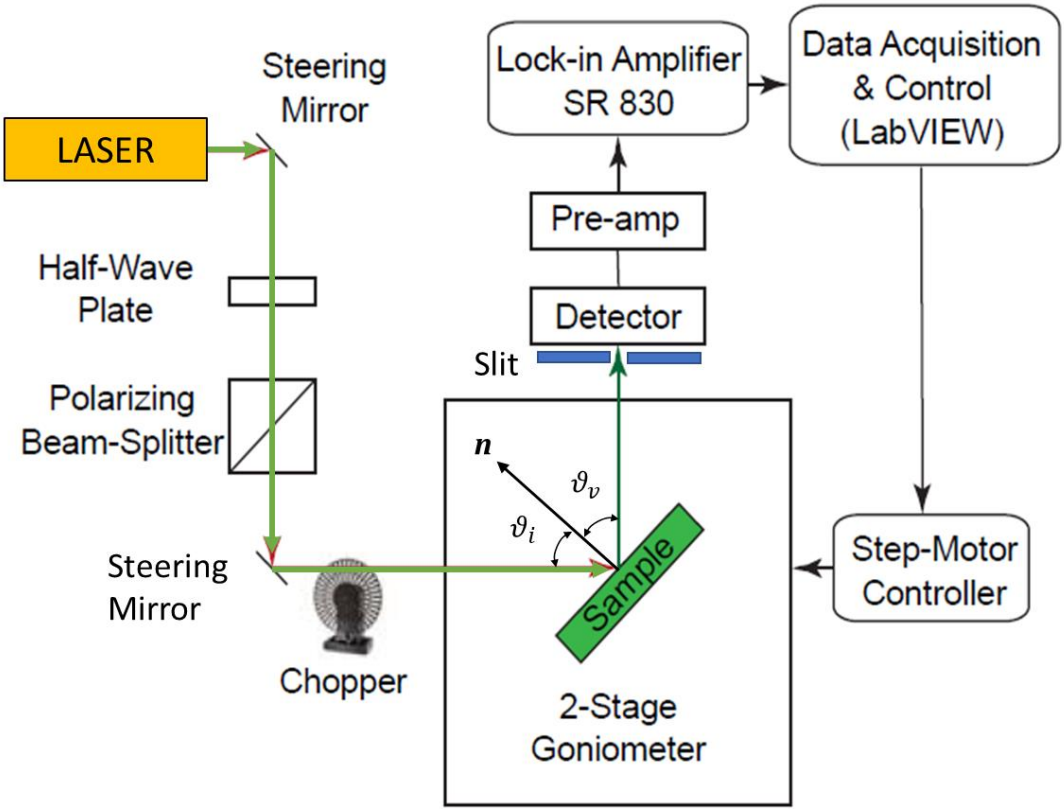

Figure 3.18 Schematic diagram of experimental apparatus [16].

3.5 BRDF Measurements using the Ultraviolet Laser (351 nm)

The Z302 samples are illuminated at their center by a power-stabilized 351-nm Ar laser. Prof. Vinh Nguyen and the author modified the experimental setup that was used for the visible light experiment to obtain new measurements for the glossy or shiny new sample of Z302

(named G1). Before working with sample G1, shown in Fig. 3.19, the earlier rough sample of Z302 (sample A) was measured for p-polarization. The scans were made first for p-polarization followed by s-polarization of the laser beam. The results observed looked promising and confirmed that the new sample created has the desired thickness, topography and uniformity. The incidence angles of the beam were 10, 20, 30, 40, 45, 50, 60, 70, 75, 80 and 85 deg. There is a trade-off between angular resolution and signal strength for the detector slit size.

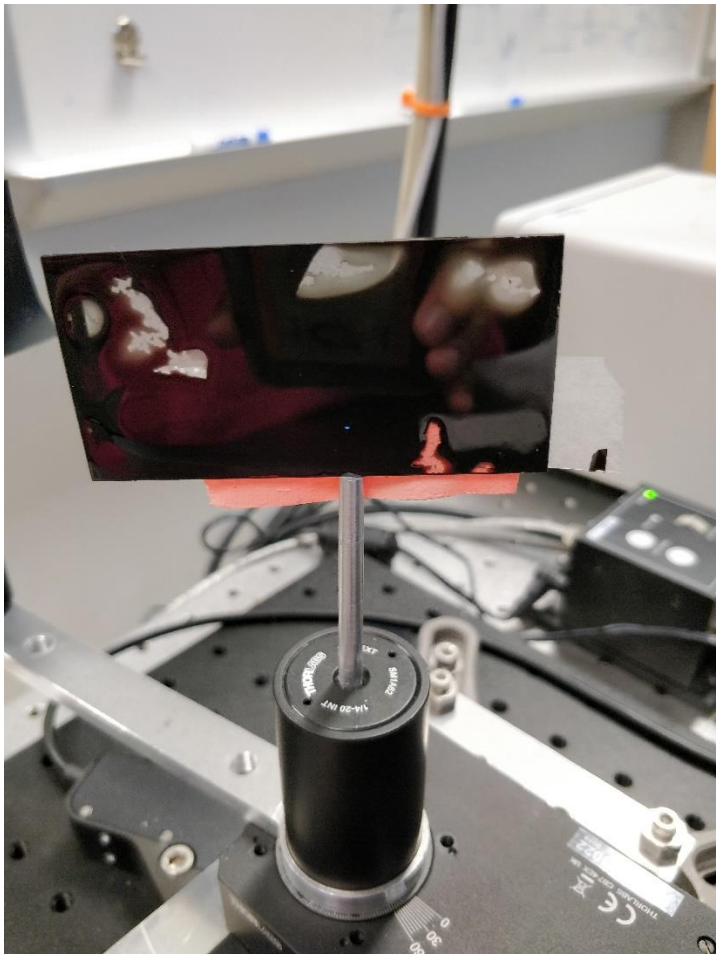

Figure 3.19 Sample G1 (glass slide with Z302 coating) mounted on setup. Small blue dot on sample is the UV laser beam.

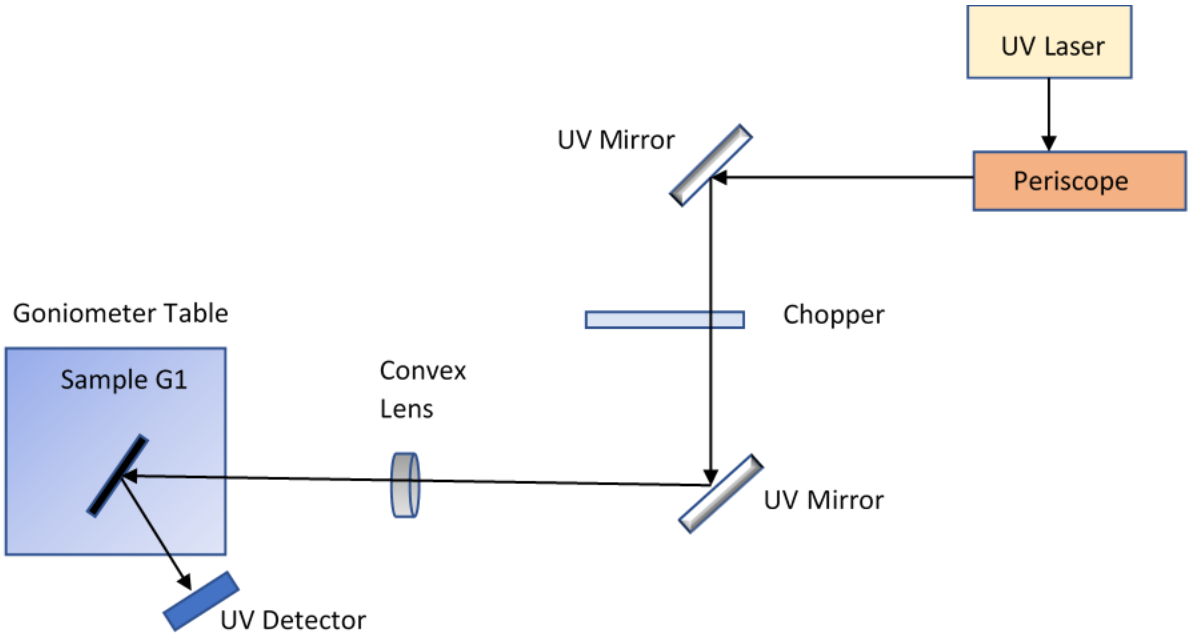

Figure 3.20 Schematic diagram for p-polarization measurement with the UV laser.

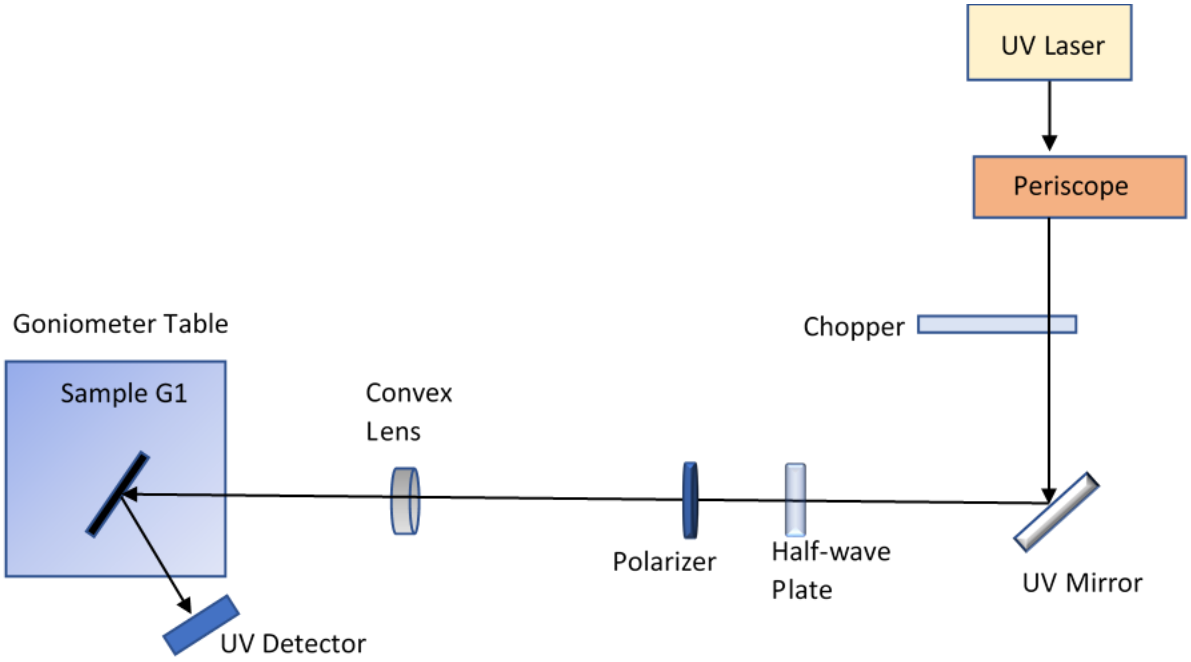

Figure 3.21 Schematic diagram for s-polarization measurement with the UV laser.

Chapter 4

Results and Discussion

This chapter presents the experimental results of the BRDF measurements described in the previous chapter and includes a discussion of the inferences drawn from them.

4.1 Incidence Angle Range

The incidence angles in the BRDF measurements were varied from 10 to 80 deg. It is not practical in the experiment to have incidence angles less than 10 deg or greater than 80 deg. For less than 10 deg the reflected beam is almost impossible to detect separately from the incident beam. For more than 80 deg the area illuminated by the incident beam on the sample is no longer circular but rather becomes elliptical, as shown in Fig. 4.1. Also, it no longer remains in the center of the sample. Both of these effects lead to inaccuracy in the BRDF measurements.

4.2 Further Remarks on the Z302 sample fabrication

1. One inference that can be drawn from the Z302 spray-application process, discussed in Chapter 2, is that multiple re-coats of Z302 as well as the dipping process both produce a smooth and uniform coat on silicon and glass coupons.

2. An important lesson that we learned for the Z302 samples is to make larger-area samples than those described in Chapter 2. This is because for Sample B (with three re-coats) the coating tended to build up at the edges of the silicon coupon. This effect of surface tension creates a visible contour on the sample that dips in the center and rises on the sides. This contour in the coating center can be avoided if the edges are farther away from the center; that is, if the coupon is larger, so that its center remains flat.
3. Z302 does not "wet" silicon and glass surfaces, which is apparent in Fig. 2.20 for the dipping method of sample fabrication.
4. In the current effort, Sample B (with three recoats of Z302, by spray application) and Sample G1 (single coat by dipping method) displayed the highest specularity characteristics when illuminated with different laser sources.

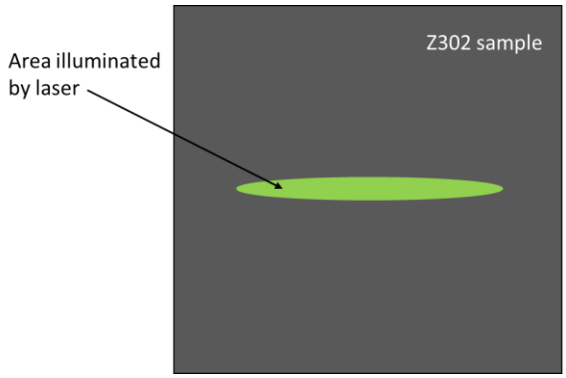

Figure 4.1 Elliptical area illuminated by the laser on the Z302 sample for angles of incidence greater than 80 deg (not to scale).

4.3 Experimental Results obtained using the Visible Laser (532 nm)

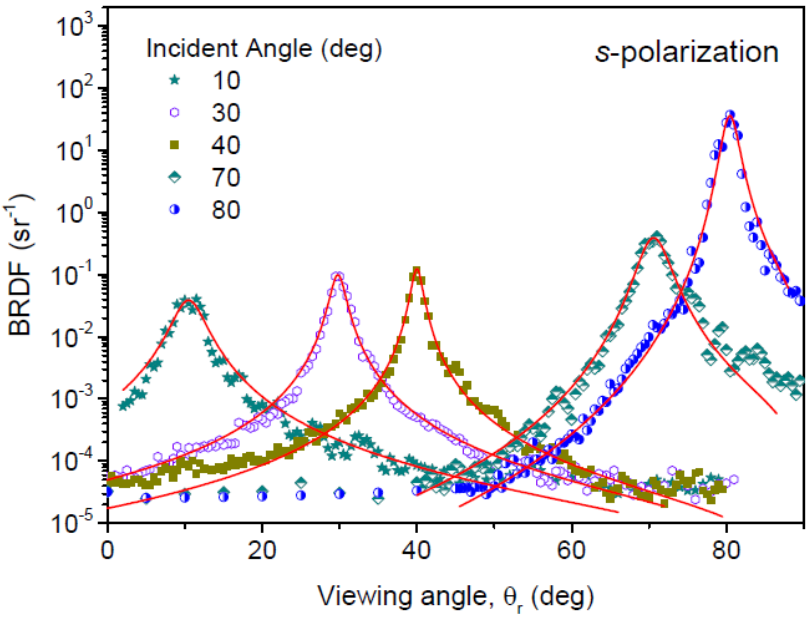

Figure 4.2 BRDF measurement results (symbols) for Z302 Sample A at 532 nm incident wavelength for s-polarization at 10, 30, 40, 70 and 80 deg angles of incidence, and a two-component BRDF model fit (curves) to the data [16].

Figure 4.2 presents the BRDF measurement results for Sample A for incidence angles of 10, 30, 40, 70 and 80 deg for s-polarization, and Figure 4.3 presents the results for p-polarization [16]. The ordinates of both figures have the same scale for easier direct comparison of results for the two polarizations. The BRDFs in the viewing angle (ϑ_r) range surrounding the specular reflection peaks are the main interest of our investigation, and this determined the data collection intervals for our measurements. The wavelength intervals adopted for viewing angles are 0.5, 0.2 and 0.05 deg near the specular reflection angles, whereas 5 deg intervals are used for off-specular range reflection angles. Reflection intensities

at each viewing angle have been averaged over three observations in order to reduce random error. The standard deviation near the specular peaks is estimated to be within ±5 percent, and for very small BRDF values it is estimated to be ±30 percent. The latter value is due to the low signal-to-noise ratio occurring at the base of the BRDF curves. The BRDFs for Sample B at 80 deg angle of incidence for both s- and p- polarizations are presented in Fig. 4.4.

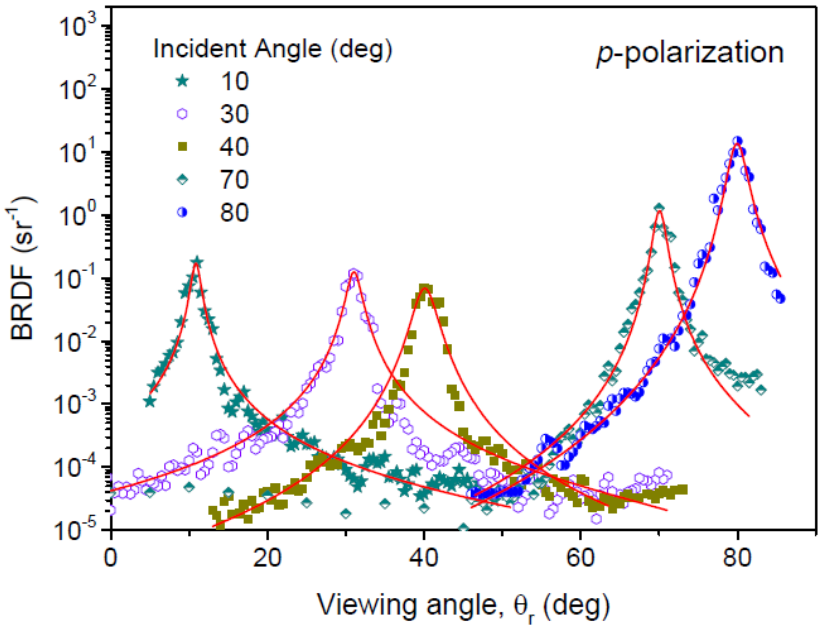

Figure 4.3 BRDF measurement results (symbols) for Z302 Sample A at 532 nm incident wavelength for p-polarization at 10, 30, 40, 70 and 80 deg angles of incidence, and a two-component BRDF model fit (curves) to the data [16].

From Figs. 4.2, 4.3 and 4.4, it can be observed that the BRDFs as well as the specular peaks at $\vartheta_r = \vartheta_i$ have different shapes and magnitudes depending on the sample and polarization of incident light. The shapes of the specular peaks in the BRDFs of these two samples are consistent with the appearance and roughness of their surfaces, as shown in Fig. 2.15. The BRDFs of Sample B are comparable in shape and magnitude to Z302 measurements reported

in Reference 13. For sample A, the measured BRDFs decrease from the peak to the smallest values by about six orders of magnitude for an 80-deg angle of incidence. For sample B, the peak values at large reflection angles are greater than Sample A by more than one order of magnitude. Also, the peaks are attenuated and broader due to scattering from the rough surface of Sample A. This indicates that sample A is more diffuse in terms of light scattering. The magnitudes of peaks for s-polarization are higher than those for p-polarization for these samples. Also, for p-polarization, as seen in Fig. 4.3, the intensity of peaks in the BRDFs decreases from the normal incidence, that is 0 deg, to about 60 deg, followed by an increase by several orders of magnitude as the incidence angle increases. This observation is in agreement with the Fresnel equation for a smooth electrically conducting interface.

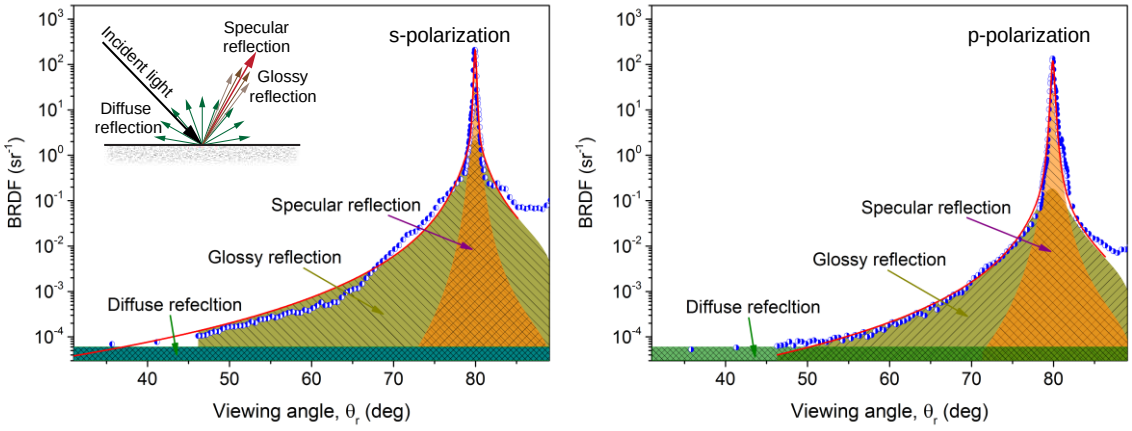

Figure 4.4 BRDF measurement results for Sample B at 532 nm and at 80 deg angle of incidence for both s-polarization (left) and p-polarization (right). A deconvolution of a three component BRDF fit is shown for the glossy, specular and diffuse reflection components. These components are illustrated in the inset [16].

4.4 Experimental Results obtained using the UV Laser (351 nm)

Figure 4.5 presents the BRDF measurement results for Sample G1 for incidence angles of 10, 20, 30, 40, 50, 60, 70 and 80 deg for both p- and s-polarizations at 351 nm [20]. The dip observed in the p-polarization is similar to the visible wavelength results. This dip, in agreement with classical optics, occurs at the Brewster angle, which is about 50 deg in our case [25, p. 708]. The peaks in the BRDFs for s-polarization increase with incidence angle, similar to the behavior observed in visible light results. Unpublished BRDF test data at 633 nm [15] recently released by NASA are plotted in Fig. 1.4. The trends in Fig. 4.5 and Fig. 1.4 are very similar. However, a difference can be observed in the peak and background values in the two data sets, with the values in Fig. 4.5 being uniformly lower than corresponding values in Fig. 4.6 by slightly greater than an order of magnitude. This difference may be due to the wavelength dependence of Z302 BRDF. The Photon Engineering measurements were made with reference to a standard sample of known reflectivity, whereas our measurements are absolute, which could also explain the difference. Note that the polarized BRDF data in Fig. 4.5 can be converted to equivalent unpolarized data by averaging the s- and p-polarization values at the corresponding viewing angles.

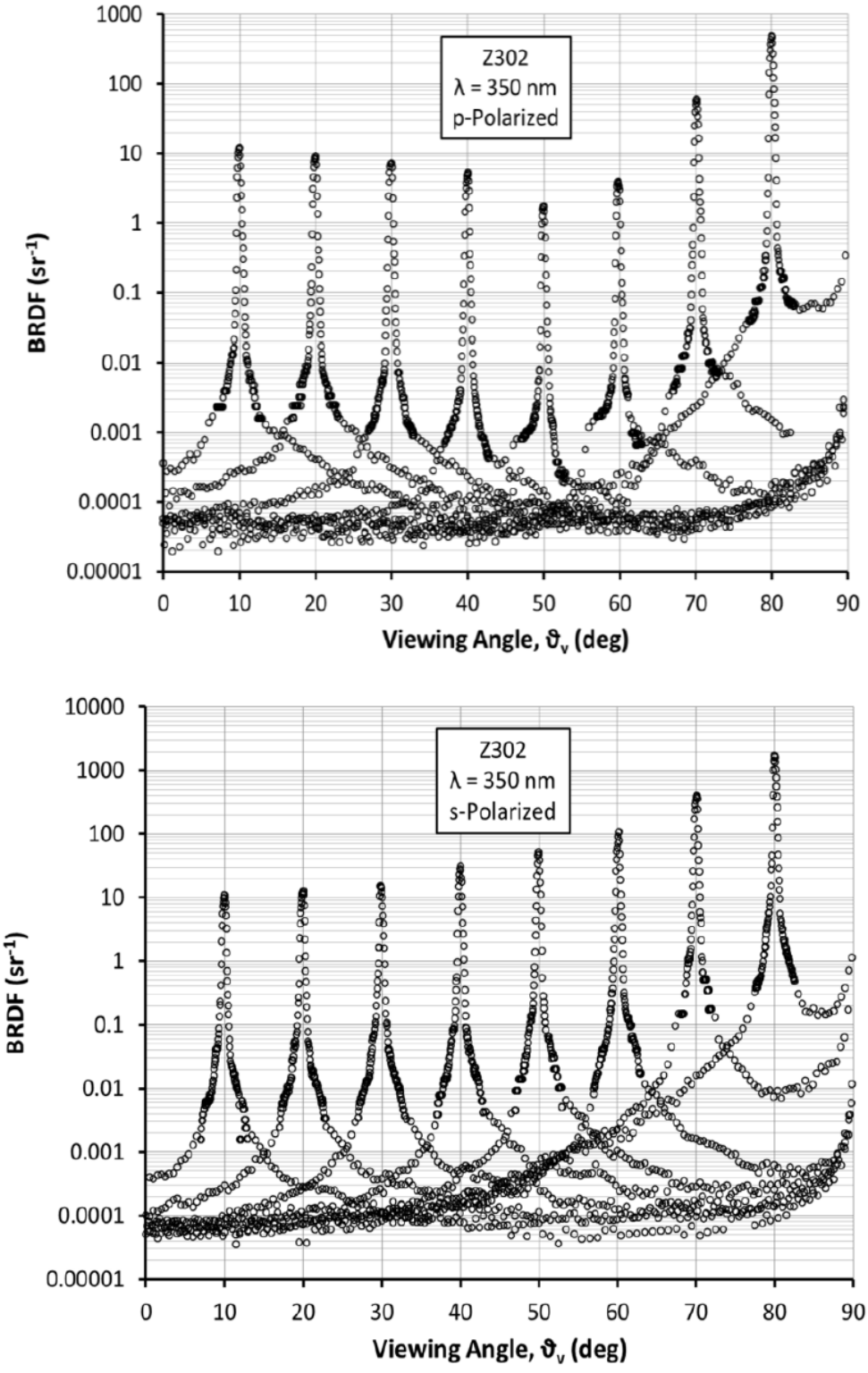

Figure 4.5 BRDF measurement results for Sample G1 at 351 nm at 10, 20, 30, 40, 50, 60, 70 and 80 deg for both p- and s-polarizations [20].

Chapter 5

Future Work and Conclusions

This chapter presents conclusions drawn from this effort and presents recommendations for future research.

5.1 Conclusions

From the effort reported in this thesis we may conclude the following:

- An experimental investigation of the bidirectional reflectance distribution function (BRDF) for absorptive coating Aeroglaze Z302 is presented.
- An automated goniometer reflectometer designed and implemented to measure the BRDF of Z302 and is capable of measuring similar coatings.
- Measurements are reported for both p- and s-polarizations. We believe this is the first report of BRDF measurements for Z302 with polarized light and in the ultraviolet.
- The results are in reasonable agreement with those reported in the literature and are in qualitative agreement with previously unpublished results provided by NASA.
- The results are consistent with theoretical expectations and are amenable to interpretation based on the observed degree of surface roughness.

5.2 Recommendations

The following recommendations are made for future effort:

- Z302 samples should be created with more uniform surface texture over a larger area.
- The factors that result in the BRDF measurement variations across the reports cited should be further investigated, specifically the difference in BRDF amplitudes observed in Figs. 4.5 and 1.4.
- BRDF measurements should be performed in the infrared wavelength region.

References

[1] Mahan, J. Robert, *The Monte Carlo Ray-Trace Method in Radiation Heat Transfer and Applied Optics*, Wiley (2018).

[2] *Chembar Inc.* Retrieved July 5, 2018, from https://www.chembar.com/product/lord-aeroglaze-z302-absorptive-polyurethane-black/

[3] Poulson, Richard E., Test methods in spectrophotometry: Stray-light determination, *Applied Optics*, **3**(1), pp. 99-104 (1964).

[4] Newkirk, G. and Bohlin, D., Reduction of Scattered Light in the Coronagraph, *Applied Optics*, **2**(2), pp. 131-140 (1963).

[5] Persky, M. J., Review of black surfaces for space-borne infrared systems, *Review of Scientific Instruments*, **70**(5), pp. 2193-2217 (May 1999).

[6] *K & K Associates.* Retrieved September 4, 2018, from http://www.tak2000.com/data/finish.htm#Black

[7] Mahan, J. Robert, *Radiation Heat Transfer: A Statistical Approach,* Wiley (2002).

[8] Chao Qi, Chun-ling Yang, Jing-min Dai, Guo-liang Zhao, "Study on the BRDF application", *Proceedings of SPIE 6595, Fundamental Problems of Optoelectronics and Microelectronics III,* **659547** (5 March 2007).

[9] Andrews, Rob W., Andrew Pollard, and Joshua M. Pearce, "Photovoltaic system performance enhancement with non-tracking planar concentrators: Experimental results and BDRF based modelling." *Photovoltaic Specialists Conference (PVSC), 2013 IEEE 39th*. IEEE, 2013.

[10] Elena Georgieva, Kory J. Priestley, Barry Dunn, Richard Cageao, Anum Barki, Jim Osmundsen, Craig Turczynski, and Nural Abedin, "Radiation Budget Instrument (RBI) for JPSS-2," 24th Conference on Characterization and Radiometric Calibration for Remote Sensing (CALCON), Space Dynamics Laboratory, Utah State University, Logan UT, August 20-24, 2015.

[11] Wielicki, B. A., R. D. Cess, M. D. King, D. A. Randall, and E. F. Harrison, "Mission To Planet Earth: Role of Clouds and Radiation in Climate," **Bulletin of the American Meteorological Society**, **76** (11), November 1995, pp. 2125-2153.

[12] *Clouds and the Earth's Radiant Energy System.* Retrieved November 28, 2018, from https://ceres.larc.nasa.gov/

[13] Prokhorov, A., and N. I. Prokhorova, Application of the three-component bidirectional reflectance distribution function model to Monte Carlo calculation of the spectral effective emissivities of nonisothermal blackbody cavities, *Applied Optics*, **51**(33), pp. 8003-8012 (November 20, 2012).

[14] Mahan, J. R., N. Q. Vinh, and K. J. Priestley, An application of the Monte Carlo ray-trace method with bidirectional reflection, *Paper TFEC-2018-22038, 3rd Thermal and Fluids Engineering Conference* (March 4-7, 2018).

[15] Shure, Mark, RBI Z302 BRDF Test Data with Unlimited Rights, Harris Space and Intelligence Systems Memo RBI-18-182 to Dr. Kory J. Priestley, NASA LaRC (October 3, 2018).

[16] Shirsekar, Deepali, Yifei Wang, J. Robert Mahan, Kory J. Priestley, and Vinh Q. Nguyen, Bidirectional reflectance measurement of black absorber layers for use in optical instrument design, *Proceedings of SPIE, Optical Modeling and Performance Predictions X*, **10743**(03), pp. 1-7 (September 17, 2018).

[17] *Pexa.* Retrieved November 27, 2018, from http://www.pexa.com/products/space_optical_coatings/

[18] *Lord Corporation.* Retrieved November 25, 2018, from https://www.lord.com/products-and-solutions/coatings

[19] *MatWeb, LLC.* Retrieved November 25, 2018, from http://www.matweb.com/search/datasheet.aspx?matguid=c5705ec1baca439cbe4cf122276fe5f9&n=1

[20] Shirsekar, Deepali, Vinh Q. Nguyen, J. Robert Mahan, Kory J. Priestley, Design and demonstration of an automated bidirectional reflectometer for low-reflectivity optical coatings, *Paper TFEC-2019-27537, 4th Thermal and Fluids Engineering Conference* (April 7-9, 2019). Full paper accepted for publication in **Proceedings of the ASTFE**.

[21] Shen, Y. J., Zhu, Q. Z., & Zhang, Z. M., A scatterometer for measuring the bidirectional reflectance and transmittance of semiconductor wafers with rough surfaces, *Review of scientific instruments*, **74**(11), pp. 4885-4892 (2003).

[22] *Wikipedia*. Retrieved December 1, 2018, from https://en.wikipedia.org/wiki/Optical_chopper

[23] *Onset ELECTRO-OPTICS CO., LTD.* Retrieved November 25, 2018, from http://www.onset-eo.com/en/product_details.php?cde=PDT510fdbe8453e1

[24] *SRS.* Retrieved November 25, 2018, from https://www.thinksrs.com/downloads/pdfs/applicationnotes/AboutLIAs.pdf

[25] Shiffer, Ralf, Reflectivity of a slightly rough surface, *Applied Optics*, **26**(4), pp. 704-712 (February 1987).